Journal of Thermal Analysis and Calorimetry (2022) 147:6035–6071
https://doi.org/10.1007/s10973-021-10876-2

A review on correlations of bubble growth mechanisms and bubble dynamics parameters in nucleate boiling

Mahyar Ghazivini[1] · Mazen Hafez[1] · Abhishek Ratanpara[1] · Myeongsub Kim[1]

Received: 31 December 2020 / Accepted: 28 April 2021 / Published online: 4 July 2021

Abstract

The benefits of nucleate pool boiling phenomena and their potential applications on thermal management of various microelectronic devices have triggered the development of new approaches that augment the magnitude of heat transfer rate. To implement these approaches, an accurate estimation of the boiling heat transfer coefficient between the fluid and the heated surface is often required. The acquisition of the boiling heat transfer coefficient must follow a better understanding of the bubble ebullition cycle because of its inherent coupling with heat transfer mechanisms involved in this cycle. Bubble ebullition occurs by periodic bubble nucleation on a boiling surface, bubble growth, and subsequent bubble departure from the surface. Different parameters related to the dynamics of the bubble ebullition cycle, including bubble departure diameter, bubble waiting period, active nucleation site density, bubble growth period, bubble departure frequency, and bubble growth rate govern the heat transfer rate in the nucleate pool boiling. Thus, numerous empirical correlations that determine the boiling heat transfer coefficient have been proposed by many researchers according to different bubble dynamics parameters. To accurately predict the boiling heat transfer coefficient and boiling heat flux based on the bubble ebullition cycle, understanding bubble growth mechanisms and associated dominant parameters is crucial. In this review, different bubble growth mechanisms during nucleate pool boiling are thoroughly reviewed. Then, bubble dynamics parameters used in different correlations for determining the boiling heat transfer coefficient are discussed. Semi-empirical and empirical correlations for determining these parameters are also extensively provided. Additionally, a detailed review of factors affecting bubble dynamics parameters is provided. Next, different applications of nucleate boiling in cooling systems are reviewed. Overall, this review includes various correlations from experimental and numerical data, which can be used to better predict the heat transfer during nucleate boiling.

Keywords Bubble growth · Nucleate boiling · Bubble dynamics parameters · Cooling systems

Abbreviations

A	Area of heated surface (m^2)
C_p	Specific heat (kJ kg^{-1} $°C^{-1}$)
C_D	Drag coefficient
D_d	Bubble departure diameter (m)
D	Bubble diameter (m)
D_c	Cavity diameter (μm)
dD/dt	Bubble growth rate
f	Bubble departure frequency (1 s^{-1})
g	Gravitational acceleration (m s^{-2})
h	Heat transfer coefficient (W $m^{-2}K^{-1}$)
h_{lv}	Latent heat of vaporization (J kg^{-1})
Ja	Jakob number ($\rho_l C_{pl}(T_w - T_{sat})/\rho_v h_{lv}$)
k	Thermal conductivity ($W/m^{-1}K^{-1}$)
Nu	Nusselt number (hD k^{-1})
N	Number of nucleation sites
n_s	Active nucleation site density (sites m^{-2})
$\overline{n}_a$	Average cavity density (sites m^{-2})
P	Pressure (MPa)
Pr	Prandtl number ($\mu_l C_{pl}/k_l$)
R_a	Surface roughness (μm)
R_c	Cavity radius (μm)
R_c^+	Non-dimensional critical cavity radius
r	Bubble radius (m)
r_b	Radius of the liquid microlayer under bubble (m)
r^+	Non-dimensional bubble radius
T	Temperature (K)
t	Time (s)
t_w	Bubble waiting period (s)
t_g	Bubble growth period (s)

✉ Myeongsub Kim
kimm@fau.edu

[1] Ocean and Mechanical Engineering, Florida Atlantic University, 777 Glades Rd, Boca Raton, FL 33431, USA

t^+ Non-dimensional time
V Volume (m^3)
V_d Bubble departure volume

Greek Letters

θ Contact angle (°)
ρ Density (kg m^{-3})
Δ Difference
ϕ Dimensionless surface roughness parameter
μ Dynamic viscosity (kg m^{-1} s^{-1})
$\underline{\beta}$ Half cone angle (°)
$\overline{\beta}$ Mean half cone angle (°)
ν Kinematic viscosity (m^2 s^{-1})
σ Surface tension (N m^{-1})
δ Thermal boundary layer thickness (m)
α Thermal diffusivity ($k_l/\rho_l C_{pl}$)(m^2 s^{-1})
ε Volumetric expansion coefficient (K^{-1})

Superscripts

$+$ Non-dimensional

Subscripts

C Cavity
L Liquid phase
Max Maximum
Min Minimum
Nc Natural convection
B Boiling
Sat Saturation condition
Tc Transient conduction
S Heating surface
v Vapor phase

Introduction

The exponential growth in component density of microelectronic devices has demanded innovative cooling methodologies to manage a high magnitude of heat fluxes [1–4]. Nucleate boiling has been extensively utilized as an efficient cooling strategy due to the high heat transfer coefficient between liquid and solid for low superheats [5]. Various domestic and industrial applications that involve high-power electronics utilize nucleate boiling for high heat removal [6, 7]. Therefore, understanding the nucleate boiling process is of great importance to further improve the heat removal capacity while advancing this strategy to numerous applications [8]. Even though different investigations regarding nucleate boiling have been performed over recent years, numerous ambiguities related to the boiling process still exist. This is mainly due to the high complexity of the boiling process, which involves intermingled phenomena including contact line dynamics, liquid–vapor phase change, unsteady temperature gradients, and turbulent flows [8]. To better understand, a majority of the investigations on nucleate boiling have been concentrated on the bubble ebullition cycle, which consists of the continuous incident of bubble nucleation on a heated surface, bubble growth, and bubble departure from the surface. During the bubble ebullition cycle, the total heat transfer from the heated surface to the fluid can be estimated as $\sim nq_{single}$ where n indicates the nucleation site density and q_{single} is an amount of heat per time transferred by a single bubble ebullition cycle. Although various approximate correlations and models have been proposed to calculate q_{single} [9–11], the emergence of computer simulations and elaborated experiments have enabled researchers to better understand the bubble cycle and accurately obtain relevant data [12–14]. These advanced simulations and experiments have revealed that heat transfer mainly takes place by either means of the liquid–vapor interface through the microlayer or from the bulk surrounding liquid [15].

Four heat transfer regimes in pool boiling

The boiling curve, as shown in Fig. 1, is extensively used for describing mechanisms and regimes of pool boiling heat transfer [16, 17]. In this curve, the changes of heat flux from a surface to surrounding liquid are correlated with wall superheat defined as a difference between wall and liquid saturation temperature [18–21]. This curve differentiates four unique regimes of heat transfer at distinct levels of wall superheat [22–24]. These regimes include (1) a single-phase (liquid) regime associated with low superheat, (2) a nucleate boiling regime contributed to bubble nucleation at the

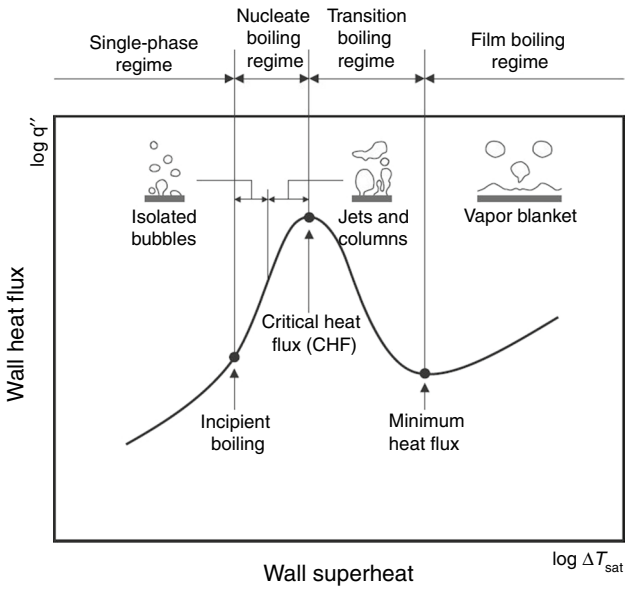

Fig. 1 Pool boiling curve that shows the relationship between heat flux and associated wall superheat ($\Delta T = T - T_{sat}$) [25]

surface, (3) a transition boiling regime in which parts of the surface experience bubble nucleation, whereas the rest are blanketed with vapor, (4) a film boiling regime associated with high wall superheat resulting in vapor blanketing the entire surface. Three crucial transition points delimitate these four regimes: (1) incipient boiling (onset of boiling) associated with forming the first bubble on the surface, (2) the critical heat flux in which localized vapor blankets replace bubble nucleation by joining together throughout the surface, and (3) a Leidenfrost point (minimum heat flux) where breakup in the uninterrupted vapor blanket starts during film boiling while reducing wall superheat. Additionally, the highest and lowest heat transfer coefficients can be estimated based on the boiling curve and transition points, belonging to the nucleate boiling and film boiling regimes, respectively.

Among these four regimes, the nucleate boiling is considered as the most influential regime in practical heat transfer applications. Since the nucleate boiling regime consists of the continuous bubble ebullition cycle which leads to continuous heat transfer, a comprehensive understanding of bubble formation and its impacts on heat transfer is crucial. Therefore, a basic background on nucleate boiling and associated time-dependent mechanisms of bubble formation will be discussed in the succeeding sections.

Background on nucleate boiling

In nucleate boiling, bubble nucleation is considered as the first stage of the bubble ebullition cycle. Based on trapped vapor theory, air bubbles are trapped by cavities on the surface where these trapping sites work as nucleation sites [26]. During bubble growth, the vapor pressure inside the bubble is higher than the pressure of the surrounding liquid as a result of the convex curvature of trapped vapor bubbles in cavities. When the temperature of the surrounding liquid equals the saturation temperature, its equilibrium vapor pressure does not match the vapor pressure inside the trapped bubble. Nonetheless, in the condition of sufficiently superheated liquid, its equilibrium vapor pressure is higher than the bubble vapor pressure that induces bubble growth. Based on Young–Laplace and Clausius–Clapeyron equations, the specific condition that leads to bubble growth or nucleation takes place when the chemical potentials (e.g., specific volume, enthalpy, and saturation temperature) of the vapor and the liquid match [27]:

$$\Delta T \approx \frac{2\gamma_{\mathrm{lv}} T_{\mathrm{sat}} \upsilon_{\mathrm{fg}}}{h_{\mathrm{fg}} R_{\mathrm{b}}} \tag{1}$$

When bubble nucleation occurs, the superheat could be measured by determining the radius of curvature of a nucleation site (R_{b}) in Eq. (1). Lorenz and Hsu models are the two prevalent methods for determining the bubble radius of curvature [28, 29]. The radius of curvature is obviously associated with the cavity radius; however, it is not necessarily required to be identical with the cavity radius. For a specific cavity and liquid, R_{b} could be smaller than, equal to, and larger than cavity radius, relying on the vapor volume.

Not only the radius of curvature but also the force balance during bubble growth is another important factor that affects the nucleate boiling. During bubble nucleation, multiple forces including buoyancy, shear forces at the interface, pressure difference between vapor and liquid, surface tension, and gravitational forces play a critical role in nucleate boiling. In nucleate boiling, when the buoyancy force overcomes the surface tension force as well as the gravitational force, the vapor bubble is detached from the heated surface while augmenting its size. The bubble size and generation frequency are the important factors to increase the heat transfer rate. Likewise, it is a prominent fact that the magnitude of heat removal rate in the nucleate boiling is a function of time-dependent parameters, called bubble dynamics parameters, including bubble departure diameter, bubble departure frequency, bubble growth period, bubble waiting period, and nucleation site density. Thus, the quantification of the bubble dynamics parameters is required to accurately determine the heat transfer rate, and this could be achieved by understanding the bubble formation, growth, and departure on the heated surface.

To determine bubble dynamics parameters, various empirical or semi-empirical correlations have been developed based on principals of boiling heat transfer, which estimate experimental data of various researchers with minimal errors [30–33]. The precision of these correlations relies on how the bubble dynamics parameters are estimated. These proposed correlations can be used to determine the boiling heat flux and boiling heat transfer coefficient. The goal of this paper is to primarily provide a detailed review of correlations for determining bubble radius during its growth and bubble dynamics parameters in nucleate boiling and secondarily to review important factors governing the bubble dynamics parameters. Hence, this paper starts reviewing different bubble growth mechanisms. Secondly, the bubble dynamics parameters used in different correlations for determining the boiling heat transfer coefficient are described and reviewed. In accordance with the information regarding the bubble dynamics parameters, a detailed review of factors affecting these parameters is provided. Overall, this review paper includes various correlations developed by different studies based on experimental and numerical data in order to better predict the heat transfer during nucleate boiling. This review could be worthwhile in developing boiling heat transfer correlations regarding bubble dynamics parameters.

Bubble growth mechanisms

Two mechanisms for bubble nucleation and subsequent growth have been reviewed. The first type is homogenous nucleation, which takes place in the bulk liquid at upper levels of supersaturation. Supersaturation is referred to a condition of which a solution contains more of a dissolved material than could be dissolved in the solvent under normal circumstances. The second mechanism is heterogeneous nucleation that occurs at surface defects such as cavities and tiny holes at lower levels of supersaturation. Although understanding these mechanisms is a crucial step to obtain accurate modeling in nucleate boiling processes, the bubble growth is inherently complicated with various forces such as surface tension, the pressure difference between the vapor and liquid, shear forces, and the inertia of the ambient liquid. Also, the bubble cycle is time-dependent, which leads to the variation of mass, momentum, energy equation over time. Nonetheless, considerable efforts have been made to promote the understanding of these processes for precise modeling, and the following sections discuss the two bubble growth mechanisms.

Homogenous bubble growth

Bubble growth in a superheated liquid is regarded as homogenous. Homogeneous bubble growth is mainly governed by inertial-controlled and heat transfer-controlled growth mechanisms at different phases during its growth. In the inertia-controlled bubble growth that is valid only in the initial stage, heat transfer is neglected. On the other hand, in the heat transfer-controlled bubble growth which is suitable only in the later stage, the influence of inertia on bubble growth is ignored. For complete modeling of bubble growth, these two growth mechanisms must be considered.

In the initial stage of bubble growth, a vapor bubble expands freely when its radius reaches an unstable equilibrium. During the early stage when the bubble radius is small, the Laplace–Young equation states that the pressure differential throughout the interface reaches its highest value. This results in great inertia terms in the momentum equation. Meantime, the interface's temperature approaches the superheat temperature of the ambient liquid. Thus, the greatest driving temperature differential is experienced by heat transfer from the liquid into the vapor bubble. Consequently, inertia or the momentum exchange between liquid and vapor limit the initial bubble growth [34].

By combining the Rayleigh, Clausius–Clapeyron, and the continuity equations under the conditions of an incompressible and radially symmetric inviscid flow, the instantaneous bubble radius in the initial stage of growth is calculated as follows: The continuity equation is expressed as

$$\frac{1}{r^2}\frac{\partial(r^2u)}{\partial r}=0 \tag{2}$$

where u is the radial velocity in the liquid phase. The following equation is obtained by integrating Eq. (2) over the interval of (R, r)

$$u(r,t)=\frac{\mathrm{d}R}{\mathrm{d}t}\left(\frac{R}{r}\right)^2 \tag{3}$$

The momentum equation for the surrounding liquid is

$$\rho_{\mathrm{l}}\left(\frac{\partial u}{\partial t}+u\frac{\partial u}{\partial r}\right)=-\frac{\partial p}{\partial r} \tag{4}$$

By substituting Eq. (3) in Eq. (4)

$$\frac{\rho_{\mathrm{l}}}{r^2}\left[2R\left(\frac{\mathrm{d}R}{\mathrm{d}t}\right)^2+R^2\frac{\mathrm{d}^2R}{\mathrm{d}t^2}\right]-\frac{2\rho_{\mathrm{l}}R^4}{r^5}\left(\frac{\mathrm{d}R}{\mathrm{d}t}\right)^2=-\frac{\partial p}{\partial r} \tag{5}$$

Integrating Eq. (5) over the interval of (R,∞), the Rayleigh equation is obtained as

$$R\frac{\mathrm{d}^2R}{\mathrm{d}t^2}+\frac{3}{2}\left(\frac{\mathrm{d}R}{\mathrm{d}t}\right)^2=\frac{1}{\rho_{\mathrm{l}}}\left[\rho_{\mathrm{l}}(R)-\rho_{\mathrm{l}}(\infty)\right] \tag{6}$$

By recalling the Laplace–Young equation ($p_{\mathrm{g}}+p_{\mathrm{v}}-p_{\mathrm{l}}=\frac{2\sigma}{R_{\mathrm{b}}}$) and substituting $p_g=0$ in Eq. (6)

$$R\frac{\mathrm{d}^2R}{\mathrm{d}t^2}+\frac{3}{2}\left(\frac{\mathrm{d}R}{\mathrm{d}t}\right)^2=\frac{1}{\rho_{\mathrm{l}}}\left[p_{\mathrm{v}}-p_{\mathrm{l}}(\infty)-\frac{2\sigma}{R}\right] \tag{7}$$

where $P_{\mathrm{v}}-P_{\mathrm{l}}(\infty)$ and σ are the pressure difference between water vapor and bulk liquid and surface tension, respectively. During the early stage of bubble growth, the surface tension ($2\sigma/R$) is negligible when compared to the pressure difference ($\rho_{\mathrm{v}}-\rho_{\mathrm{l}}(\infty)$). Also, the Clausius–Clapeyron equation is expressed as

$$p_{\mathrm{v}}-p_{\mathrm{l}}(\infty)=\frac{\rho_{\mathrm{v}}h_{\mathrm{lv}}\left[T_\infty-T_{\mathrm{sat}}\left[p_{\mathrm{l}}(\infty)\right]\right]}{T_{\mathrm{sat}}\left[p_{\mathrm{l}}(\infty)\right]} \tag{8}$$

which is used to determine the pressure difference.

Therefore, the instantaneous bubble radius is expressed as

$$R(t)=\left\{\frac{2}{3}\frac{\rho_{\mathrm{v}}h_{\mathrm{lv}}}{\rho_{\mathrm{l}}}\frac{T_\infty-T_{\mathrm{sat}}\left[p_{\mathrm{l}}(\infty)\right]}{T_{\mathrm{sat}}\left[p_{\mathrm{l}}(\infty)\right]}\right\}^{\frac{1}{2}}t \tag{9}$$

According to Eq. (9), the bubble radius depends on both pressure of the bulk liquid and the temperature difference between the saturation temperature and the temperature of the bulk liquid.

On the other hand, in the latest stage of bubble growth, it is known that the inertial force becomes negligible while the pressure difference significantly reduces (based on the Laplace–Young's equation), and the interfacial motion

becomes slower. Simultaneously, the temperature difference between the interface and the vapor inside the bubble decreases. With a lower level of these forces acting on the bubble, heat transfer governs bubble growth in this stage.

$$\frac{\partial T_1}{\partial t} + u\frac{\partial T_1}{\partial r} = \frac{\alpha_l}{r^2}\frac{\partial}{\partial r}\left(r^2\frac{\partial T_1}{\partial r}\right) \tag{10}$$

where u is achieved by Eq. (3). The boundary and the initial conditions for Eq. (10) are

$$\begin{aligned} &T(r,0) = T_1(\infty),\\ &T(R,t) = T_{\text{sat}}\left(p_{\text{v}}\right),\\ &T(\infty,t) = T_1(\infty), \end{aligned} \tag{11}$$

The energy balance at the liquid–vapor interface is

$$k_1\frac{\partial T}{\partial r}(\text{at}r = R) = \rho_{\text{v}}h_{\text{lv}}\frac{\text{d}R}{\text{d}t} \tag{12}$$

As a result, the instantaneous bubble radius in the last stage of growth can be expressed as [34]

$$R(t) = 2C_{\text{R}}\sqrt{\alpha_1 t} \tag{13}$$

where C_{R} is a constant.

For large Jakob numbers (corresponding to low pressure), C_{R} is calculated by [35]

$$C_{\text{R}} = \sqrt{\frac{3}{\pi}Ja} \tag{14}$$

For small Jakob numbers,

$$C_{\text{R}} = \sqrt{\frac{Ja}{2}} \tag{15}$$

A complete bubble growth model must contain both the inertia force and heat transfer as well as make a smooth transition between these two phases. One of the correlations that consider both inertia-controlled and heat-transfer-controlled growth was introduced by Mikic et al. [9]. The bubble radius is expressed as

$$r^+ = \frac{2}{3}\left[\left(t^+ + 1\right)^{3/2} - \left(t^+\right)^{\frac{3}{2}} - 1\right] \tag{16}$$

where,

$$r^+ = \frac{r(t)A}{B^2} \tag{17}$$

$$t^+ = \frac{tA^2}{B^2} \tag{18}$$

$$A = \left\{\frac{2\left[T_1 - T_{\text{sat}}\left(P_1\right)\right]i_{\text{lv}}\rho_{\text{v}}}{\rho_1 T_{\text{sat}}\left(P_1\right)}\right\}^{1/2} \tag{19}$$

$$B = \left(\frac{12\alpha_1}{\pi}\right)^{1/2}Ja = \left(\frac{12\alpha_l}{\pi}\right)^{1/2}\left\{\frac{T_{\text{i}} - T_{\text{sat}}\left(P_1\right)c_{p,l}\rho_1}{i_{\text{lv}}\rho_{\text{v}}}\right\} \tag{20}$$

where Ja is the Jakob number,

$$Ja = \frac{\rho_1 c_{\text{Pl}}\left[T_1(\infty) - T_{\text{sat}}\left(P_{\text{v}}\right)\right]}{\rho_{\text{v}}h_{\text{lv}}} \tag{21}$$

Jakob number is the ratio of sensible heat to latent heat absorbed (or released) during the phase change process.

Although this correlation has been widely applied for describing bubble growth from the bulk superheated liquid, its inexactness has been reported particularly within the initial stages at high superheats due to the following reasons: 1. by supposing that the linearized Clausius–Clapeyron equation could be utilized for relating temperature and vapor pressure; 2. by disregarding the surface tension effect on the internal bubble pressure; and 3. by taking into account a constant vapor density [36, 37]. To obviate this inaccuracy, some corrections have been proposed. For instance, Miyatake et al. [36] suggested to delineate the whole range of bubble growth in the superheated bulk liquid.

$$r^+ = \frac{2}{3}\left\{1 + \frac{t^+}{3}\exp\left[-\left(t^+ + 1\right)^{1/2}\right]\right\}\left[\left(t^+ + 1\right)^{3/2} - \left(t^+\right)^{\frac{3}{2}} - 1\right] \tag{22}$$

where

$$r^+ = \frac{A}{B^2}\left[r(t) - r_{\text{crit}}\right] \tag{23}$$

$$t^+ = \left(\frac{A}{B}\right)^2\left\{t - t_{\text{g}}\left[1 = \exp\left[\left(-\frac{t}{t_{\text{g}}}\right)^2\right]\right]\right\} \tag{24}$$

$$A = \left[\frac{2}{3}\frac{\Delta P_0}{\rho_1}\right]^{1/2} \tag{25}$$

$$\text{B} = \left(\frac{12}{\pi}\right)^{1/2}\left\{\frac{\left[\text{T}_1 - \text{T}_{\text{sat}}\left(\text{P}_1\right)\right]\text{c}_{\text{p,1}}\rho_1\alpha_1^{1/2}}{i_{\text{lv}}\rho_{\text{v}}}\right\} \tag{26}$$

$$r_{\text{crit}} = \frac{2\sigma}{\Delta P_0} \tag{27}$$

$$t_{\text{g}} = \frac{6r_{\text{crit}}}{A} \tag{28}$$

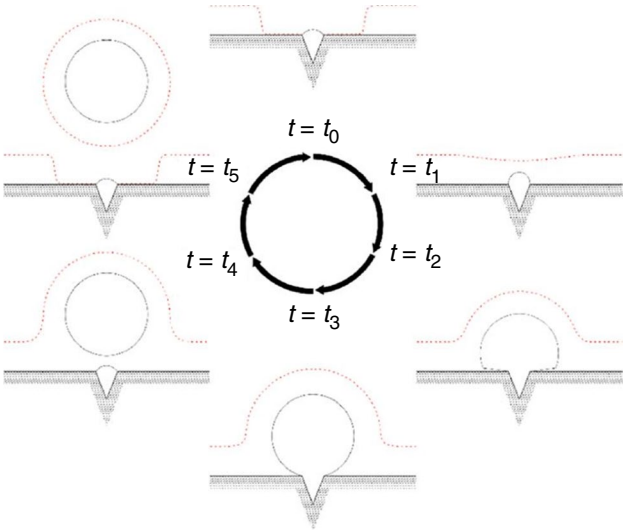

Fig. 2 Schematic of bubble growth in the cyclic model from a heated surface [40, 41]

$$\Delta P_0 = P_{\text{sat}}(T_1) - P_1 \tag{29}$$

Here, ΔP_0 and t_g are the initial pressure difference between the exterior and interior of a bubble in Pa and a bubble growth delay period in second, respectively. Additionally, Foster [38] and Zuber [39] proposed other correlations for bubble growth from a superheated liquid's layer as follows:

$$r(t) = CJa(\alpha t)^{1/2} \tag{30}$$

where $C = 2b/\sqrt{\pi}$ in Zuber [39] or $C = \sqrt{\pi}$ in Foster [38] correlations, respectively. b is a constant equivalent to 1 or $\pi/2$ and t and α are referred to the time (s) and the thermal diffusivity ($m^2 \cdot s^{-1}$), respectively.

Heterogeneous bubble growth

In heterogeneous bubble growth, growth takes place under the temperature gradient, while a vapor bubble attaches itself to a heated surface. The bubble growing procedure is repeated at a cavity on the heated surface. In this cyclic process, the bubble starts to nucleate at the cavity, depart from the cavity, and is freed up into the bulk liquid. The next bubble will be launched with the minuscule vapor left inside the cavity by releasing the former bubble from the surface. Thus, a bubble growth cycle is completed. In detail, Carey [40] modeled the heterogeneous bubble growth cycle at different stages, as shown in Figs. 2–8.

In the first stage of bubble creation, the former bubble just leaves the surface at $t = t_0$. The released bubble fractionally removes the thermal layer, which is the liquid proportion in the vicinity of the heated surface which has a higher temperature than the bulk liquid temperature. Minuscule vapor is left by releasing the former bubble, which initiates the subsequent heterogeneous nucleation process as depicted in Fig. 3. In the next period of time named "waiting period" (t_w), the thermal layer requires to be reformed, and the bubble is not growing since the heat is captured by the thermal layer. Thus, the contact between the hot surface and the liquid bulk leads to the increase in the liquid's temperature by transient conduction, therefore creating the superheated thermal layer until $t = t_1$ (Fig. 4). The bubble starts to form once the thermal layer has been reformed. At this stage, the inertia-control growth takes place, which leads to an expeditious increase in the bubble radius. The early stage of the bubble nucleation process is considerably alleviated due to the existence of a liquid microlayer between the bubble and the hot surface when compared with growth through the bulk liquid. Vaporization of the extremely thin liquid at the bubble–liquid interface considerably helps augment the

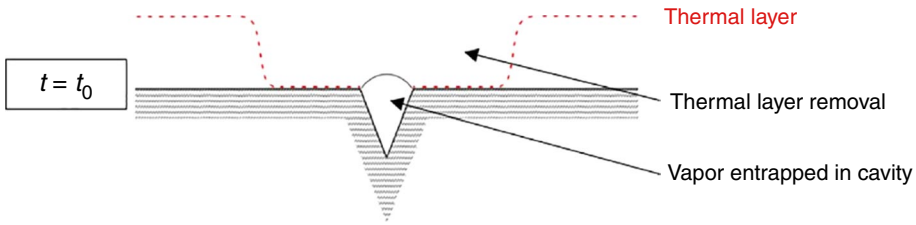

Fig. 3 Bubble growth from a heated surface: stage at $t = t_0$ [40, 41]

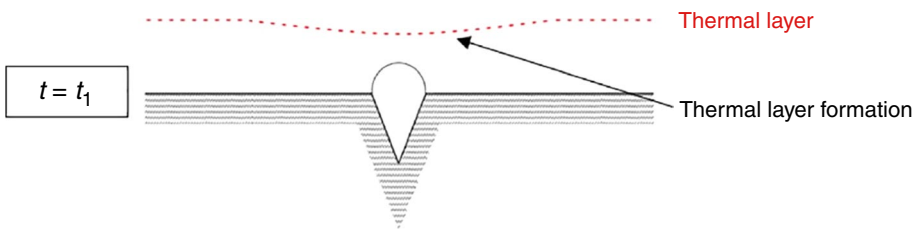

Fig. 4 Bubble growth from a heated surface: stage at $t = t_1$ [40, 41]

bubble diameter, as shown in Fig. 5. Next, the heat transfer controlled growth takes place, resulting in the formation of the bubble in a spherical shape, as shown in Fig. 6.

At the departure time at $t = t_4 = t_d$, the bubble is separated from the heated surface at its departure diameter, d_b. A small proportion of vapor from the bubble has left in the cavity that leads to the formation of the subsequent bubble by heterogeneous nucleation indicated in Fig. 7.

During the bubble departure from the heated surface, the bubble strongly magnifies the boiling heat transfer. Historically, the investigations have been centered on two important questions about nucleate boiling: first, why the highest heat transfer coefficients exist in nucleate boiling regimes, and second, how the bubble formation can be used in thermal management of electro-mechanical systems. First and foremost, at the bubble departure, the bubble removes and carries away a proportion of the thermal layer. Thus, the cold bulk liquid is combined with a significant proportion of the superheated liquid. Secondly, the bubble plays the role of energy mover: the liquid is regionally combined by stirring action. This mixed procedure is considered "sensible heat transport" or "locally enhanced convection." Afterward, due to removing a proportion of the superheated thermal layer, a part of bulk liquid with lower temperature can contact the heated surface, which results in quickly heating up the surface, named transient conduction. Ultimately, heat transfer

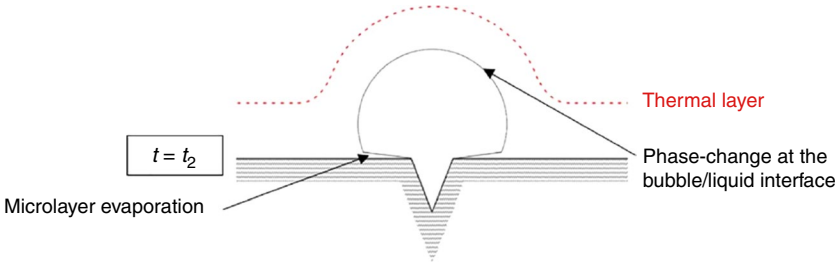

Fig. 5 Bubble growth from a surface: stage at $t = t_2$ [40, 41]

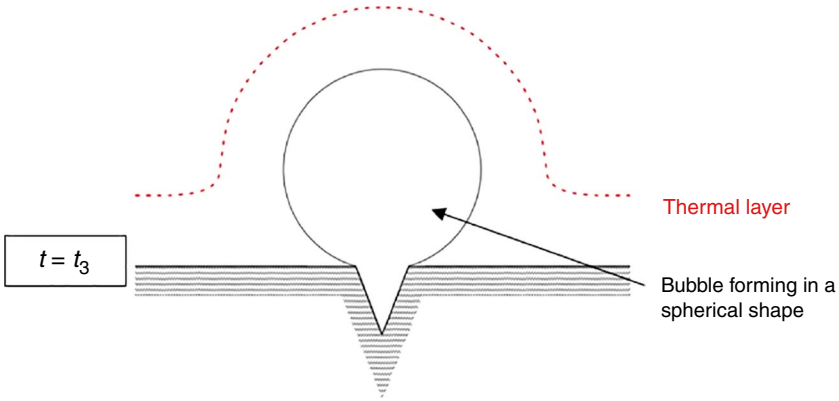

Fig. 6 Bubble growth from a surface: stage at $t = t_3$ [40, 41]

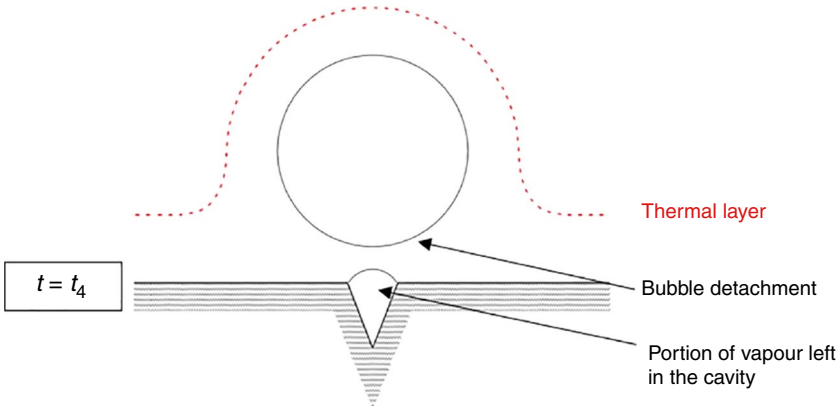

Fig. 7 Bubble growth from a surface: stage at $t = t_4$

takes place between the bubble and the nearby fluid while the entire thermal layer is moved away combined with the bulk liquid. Thus, the bubble turns to liquid when the liquid temperature is lower than the saturation point. Likewise, energy can be carried by the bubble and is transferred to the surrounding liquid by phase change, which called "latent heat transport." Figure 8 depicts the three explained mechanisms taking place at the bubble departure, which are considered the significant processes in the improved boiling heat transfer coefficients in nucleate boiling.

Lastly, the bubble can be created and reformed with the assistance of this continuous procedure, which leads to the formation of the next bubble by heterogeneous nucleation. Mikic and Rohsenow [9] are considered as two of the first scholars who developed bubble growth correlations from the heated surface. However, their model is often not recommended since it only considers heat-transfer-controlled growth and ignores the microlayer evaporation. Cole [42] developed a more accurate empirical correlation for bubble growth from a heated surface.

$$r(t) = \frac{5}{2} Ja^{3/4} (\alpha t)^{1/2} \tag{31}$$

Analogously, Cooper [42] presented,

$$r(t) = \frac{5}{2} \frac{Ja}{Pr_1^{0.5}} (\alpha t)^{1/2} \tag{32}$$

Since these correlations take into account the microlayer evaporation below the bubble, they are considered as reliable references for bubble growth from a heated surface.

It is known that the cavity size plays another important role in heterogeneous bubble growth. One of the correlation widely used in the bubble initiation, growth, and departure has been proposed by Han and Griffith [43]. They analyzed the basis of bubble nucleation and growth on a heated surface having cavities that play as a nucleation site. They observed that, when a thermal layer near the nucleation site is adequately thick, the bubble starts to grow. Under saturation conditions, they ended up finding the maximum and minimum cavity sizes generating bubbles at a given constant surface temperature.

$$(R_c)_{max,min} = \frac{\delta}{3} \left\{ 1 \pm \left[1 - \frac{12\sigma T_{sat}}{\delta \rho_v h_{lv} (T_w - T_{sat})} \right]^{\frac{1}{2}} \right\} \tag{33}$$

where δ is the thermal layer thickness.

Howell and Siegel [44] studied characteristics of bubble formation in a single cavity site with a diameter of 0.1 ~ 1 mm on a smooth surface during pool boiling. Because the bubbles grew slowly and had relatively large diameters, only buoyancy and surface tension forces were crucial at departure. When the vapor bubble expands over the liquid thermal layer ($R_c > \delta$), evaporation takes place from the fraction of the nucleus surface within the thermal layer, whereas condensation happens over the remaining fraction of the nucleus through the thermal layer. They found that the requirement for growing the vapor bubble is that the evaporative heat transfer must be higher than the amount of the condensation that ends up with the succeeding criterion,

$$T_w - T_{sat} > \frac{4\sigma T_{sat}}{\rho_v h_{lv} \delta}, \quad R_c > \delta \tag{34}$$

In case that the nucleus is confined in the thermal layer ($R_c < \delta$), the needed temperature for growing the bubble is expressed as,

$$T_w - T_{sat} > \frac{2\sigma T_{sat}}{\rho_v h_{lv} R_c} \frac{1}{1 - R_c/(2\delta)}, \quad R_c < \delta \tag{35}$$

A superior heat transfer between the heated surface and the surrounding liquid can be achieved by the bubble

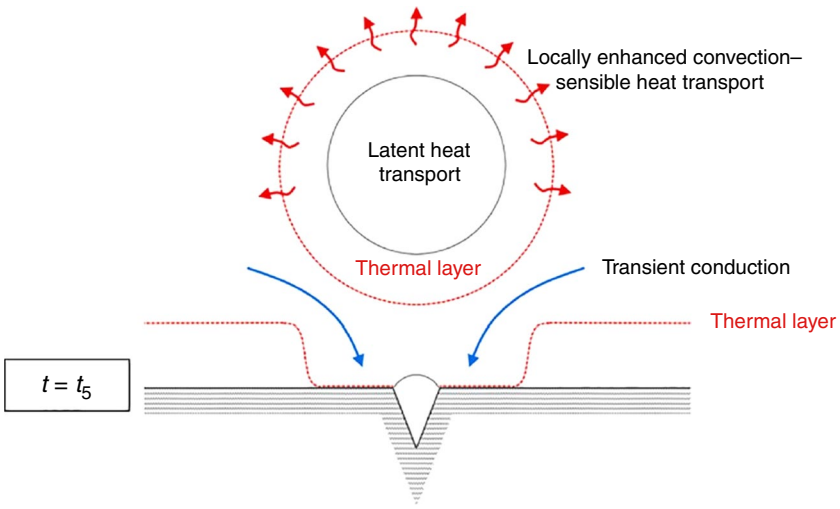

Fig. 8 Bubble growth from a surface: stage at $t = t_5$ [40, 41]

ebullition cycle. This complex heat transfer process occurs at different stages of bubble growth through unique phenomena named transient conduction, latent heat transport, and sensible heat transport. Hence, various factors called bubble dynamics parameters like departure diameter, growth rate, and frequency which deal with the bubble ebullition cycle are crucial elements to be acquired for estimating nucleate boiling heat transfer.

Bubble dynamics parameters

Bubble departure diameter (D_d)

One of the vital parameters in determining the nucleate boiling heat transfer coefficient is bubble departure diameter. By definition, the bubble departure diameter is the ultimate or equal diameter of the vapor bubble once it detaches from the heated surface during boiling [33]. Two methods, namely experimentation and force balance, are generally applied to determine the bubble departure diameter. With experimentation, images or videos of vapor bubbles during boiling are taken by a high-speed camera. Then, image processing software is used to evaluate the images, which lead to the measurement of the vapor bubble's equivalent diameter [33]. This estimation can be carried out in a nucleate boiling zone at low to modest heat flux; however, at a greater heat flux zone, the collision of multiple bubbles takes place, resulting in forming a greater bubble in size, which is not a precise measurement of the bubble departure diameter. With force balance, the bubble departure diameter can be determined prior to the departure of the bubble from the heated surface. Various forces affecting bubble growth can be enumerated, such as surface tension, drag, inertia, pressure, and buoyancy forces. Among these, surface tension and drag forces tend to prevent the bubble from detachment (negative forces), while buoyancy, inertia, and pressure forces are considered positive forces that pull the bubble from the heated surface [45]. Figure 9 shows various forces acting on a vapor bubble on a heated surface. Due to such complexity, different correlations have been developed based on experimental or non-experimental approaches to determine the bubble departure diameter. A summary of these correlations is provided in Table 1. Some correlations are simple with limited applications, and others are complicated because of the involvement of geometrical constraints.

A bubble departure diameter (D_d) correlation for pure liquid and liquid mixture has been introduced by Fritz [46], which has been broadly utilized with limited modifications.

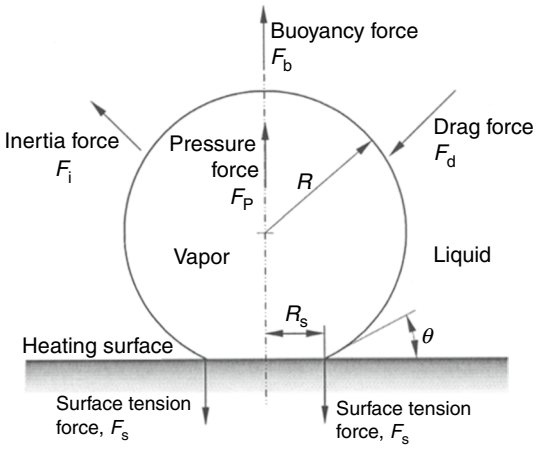

Fig. 9 Forces acting on a vapor from a heated surface [45]

$$D_d = 0.0146\theta\sqrt{\frac{2\sigma}{g(\rho_l - \rho_v)}} \tag{36}$$

where θ is 45°for water and 35°for the mixture. Fritz [46] correlated the bubble departure diameter by balancing buoyancy and surface tension forces, and this correlation is considered as the basic form of the bubble departure diameter. They correlated the bubble departure diameter with a contact angle, surface tension, and thermo-physical properties of the fluid.

In accordance with experimental investigations, Staniszewski [47] modified Firtz's correlation with taking into account the bubble growth velocity since a fast-growing bubble has a greater diameter at the moment of the departure. Additionally, Suszko and El-Genk [48] measured the bubble departure diameter, frequency, and transient growth rate in PF-5060 liquid on rough surfaces during saturation nucleate boiling by using 0.5 W cm^{-2} heat flux with a high-speed video camera. The values of bubble departure diameters on smooth copper (Cu) with an average surface roughness $Ra = 0.039$ µm and rough Cu surfaces at $Ra = 0.21$–1.79 µm were calculated to be 655 ± 40 µm and 438 ± 17 µm, respectively. Also, they proposed correlations for the departure bubble diameters on smooth (Eq. (37)) and rough Cu surfaces (Eq. (38)) as follows:

$$D_d = 234 + 81\sqrt{t_g} \tag{37}$$

$$D_d = 206 + 48\sqrt{t_g} \tag{38}$$

where t_g is the bubble growth time (ms).

Table 1 Correlations of the bubble departure diameter proposed by different researchers

No	Reference	Correlations	Condition
1	Staniszewski [47]	$D_d = 0.0071\theta\left[\frac{2\sigma}{g(\rho_l-\rho_v)}\right]^{1/2}\left[1+(0.435\frac{dD}{dt})\right]$	Pressure = 28 to 41 psi, working fluid = degassed DI water and ethanol
2	Borinshansky and Fokin [54]	$\frac{D_d}{2R_f} = -\frac{C}{2R_f} + \left[\frac{C^2}{(2R_f)^2}+1\right]^{1/2}$ $C = \left(\frac{6}{g}\right)\left(\frac{\rho_l}{\rho_l-\rho_v}\right)\left(\frac{\rho_v}{\rho_l}\right)^{0.4}\left(\frac{h}{\rho_v h_{lv}}\right), R_f = 0.0104\theta\left[\frac{\sigma}{g(\rho_l-\rho_v)}\right]^{1/2}$	–
3	Ruckenstein [55]	$D_d = \left[\frac{3\pi\rho_l\alpha_l^2 g^{0.5}(\rho_l-\rho_v)^{0.5}}{\sigma^{3/2}}\right]Ja^{4/3}\left[\frac{2\sigma}{g(\rho_l-\rho_v)}\right]^{1/2}$	–
4	Cole and Shulman [10]	$D_d = 0.0208\theta\left[\frac{\sigma g_c}{g(\rho_l-\rho_v)}\right]^{1/2}\left[1+0.0025(\frac{dD}{dt})^{\frac{3}{2}}\right]$	Pressure = 50–760 mm Hg
5	Hatton and Hall [56]	$D_d^4 g(\rho_l-\rho_v) + D_d\left[g_c\sigma D_c\sin\theta - 64\left(\frac{3\alpha_l}{\pi}\right)(Ja)^2(\frac{C_D\rho_l}{8}-\frac{\rho_l}{12}+\frac{\rho_v}{6})\right] = -g_c\sigma D_c^2$	–
6	Cole [10]	$D_d = 0.04Ja\left[\frac{2\sigma}{g(\rho_l-\rho_v)}\right]^{1/2}$	Pressure = 50–760 mm Hg
7	Cole and Rohsenow [57]	$D_d = CJa^{5/4}\left[\frac{2\sigma g_c}{g(\rho_l-\rho_v)}\right]^{1/2}$ $C = 1.5\times10^{-4}$ for water and $C = 4.65\times10^{-4}$ for others	–
8	Van Stralen and Zijl [58]	$D_d = 2.63\left(\frac{Ja^2\alpha_l^2}{g}\right)^{1/3}\left[1+\left(\frac{2\pi}{3Ja}\right)^{0.5}\right]^{1/4}$	–
9	Golorin et al. [59]	$D_d = \frac{0.0099\sigma}{g(\rho_l-\rho_v)} + \left\{\left[\frac{15.6\rho_l}{g(\rho_l-\rho_v)}\right]^{\frac{1}{3}}[0.6\alpha_l Ja]\right\}$	–
10	Kutateladze and Gogonin [60]	$D_d = 0.5(1+10^5 C)$ for $C < 0.06$ $C = \left(\frac{Ja}{\Pr}\right)\left\{\left[\frac{g\rho_l(\rho_l-\rho_v)}{\mu_l^2}\right]\left[\frac{\sigma}{g(\rho_l-\rho_v)}\right]^{3/2}\right\}^{-1}$	–
11	Kacamastafaogullari [32]	$D_d = 2.64\times10^{-5}\left[\frac{\sigma}{g(\rho_l-\rho_v)}\right]^{1/2}\left(\frac{\rho_l-\rho_v}{\rho_l}\right)^{0.9}$	The average deviation of the correlation is 33%
12	Gorenflo et al. [61]	$D_d = c(\frac{Ja^4\alpha_l^4}{g})^{1/3}\left[1+(\frac{2\pi}{3Ja})^{1/2}\right]^{4/3}$	–
13	Wenzel[62]	$D_d = 0.25\left[1+\left(\frac{Ja}{\Pr}\right)^2\left(\frac{10^5}{Ar}\right)\right]^{0.5}\left[\frac{2\sigma}{g(\rho_l-\rho_v)}\right]^{1/2}$	Applications for pure liquid and mixtures
14	Zeng et al. [63]	$D_d = 2\left\{\frac{3}{4}\left(\frac{K^{2/n}}{g}\right)\left[(\frac{3}{2})C_e n^2 + n(n-1)\right]\right\}^{\frac{n}{(2-n)}}$ K and n are determined empirically	–
15	Yang et al. [64]	$D_d = (3.0557\times10^3)\frac{\rho_l(C_{pl}T_{sat})^{0.5}\alpha\,\Pr_l^{3/5}}{\rho_v h_{lv}\eta}$ In which $\eta = \psi Ja^{0.3}, \psi = \frac{c^2}{\phi^{m-1}}\left[f(c)\right]^{\frac{2}{3}},$ $\phi = \left[1+\frac{1}{2}(\frac{\pi}{6Ja})^{\frac{2}{3}}+\frac{\pi}{6Ja}\right]$ $f(c)\approx 1-\frac{3}{4}\left[1-\sqrt{1-c^2}\right]^2+\frac{1}{4}\left[1-\sqrt{1-c^2}\right]^3,$ $c = \frac{R_b}{R_t}, m = 1.4$	Effect of gravity has not been considered
16	Lee et al. [65]	$D_d = \left(50\sqrt{27}Ja\alpha\sqrt{\frac{\rho_l}{\sigma}}\right)^2$	Constant wall temperature, Working fluids: R11 and R113
17	Jamialahmadi et al. [66]	$D_d = \left(\frac{96.75+0.01425(q)}{\ln q}\right)^{-1}$	Bulk temperature: 100–110 ºC, Salt concentration: NaCl:1–80 kg m^{-3}, Na_2SO_4:1–150 kg m^{-3}, KNO_3:1–100 kg m^{-3}
18	Kim and Kim [67]	$D_d = 0.1649\left[\frac{\sigma}{g(\rho_l-\rho_v)}\right]^{1/2}Ja^{0.7}$	DI water and R113 as working fluid

Table 1 (continued)

No	Reference	Correlations	Condition
19	Fazel and Shafaee [68]	$D_d = 40\left[\frac{\mu_v\left(\frac{q}{h_{lv}\rho_v}\right)}{\sigma\cos\theta}\right]^{1/3}\left[\frac{\sigma}{g(\rho_l-\rho_v)}\right]^{1/2}$	–
20	Phan et al. [69]	$D_d = \left(6\sqrt{\frac{3}{2}}\right)^{1/3}\left(\frac{\rho_l}{\rho_v}\right)^{-1/2}\left(\frac{\rho_l}{\rho_v}-1\right)^{1/3}\tan\theta^{-1/6}\left[\frac{\sigma}{g(\rho_l-\rho_v)}\right]^{1/2}$	Focused on the effect of contact angle
21	Nam et al. [12]	$D_d = \sqrt{\frac{24(\sin\theta)^2}{(2+3\cos\theta-(\cos\theta)^3}}\left[\frac{\sigma}{g(\rho_l-\rho_v)}\right]^{1/2}$	Working fluid: DI water. Cu nanostructure surface used as a surface
22	Lamas et al. [70]	$D_d = \sqrt{0.0027\left(\frac{\rho_l C_{pl}\Delta T}{\rho_v h_{lv}}\right)^{0.148}\left(\frac{\rho_l}{\rho_v}\right)^{-0.024}e^{0.027\theta}\left[\frac{\sigma}{g(\rho_l-\rho_v)}\right]}$	Working fluids: water, R134a, ammonia and R123, pressure: 0.1–10 bar. Contact angle: 10°–80°
23	Hamzenkhani et al. [71]	$D_d = \sqrt{\left(\frac{\sigma}{\Delta\rho g}\right)\left(\frac{\mu_v V_b}{\sigma\cos\theta}\right)^{0.25}\left(\frac{\rho_l C_{pl}\Delta T}{\rho_v h_{lv}}\right)^{0.775}\left[\frac{g\rho_l\Delta\rho}{\mu_l^2}\left(\frac{\sigma}{g\Delta\rho}\right)^{1.5}\right]^{0.05}}$	Working fluids: pure water, ethanol, ethanol/water, NaCl/water and Na_2SO_4/water
24	Suszko and El-Genk [53]	$D_d = 234 + 81\sqrt{t_g}$ $D_d = 206 + 48\sqrt{t_g}$	PF-5060 liquid on rough Cu surfaces
25	Bovard et al. [72]	$D_d = c_0\left[c_1 + Ja^{c_2}Ca^{c_3}\left(\frac{\alpha_f}{\alpha_s}\right)^{c_4}\right]\left[\frac{\sigma}{g(\rho_l-\rho_v)}\right]^{1/2}$ $c_0 = 17.952177, c_1 = 0.0172742, c_3 = 1.285607, c_3 = 0.661205, c_4 = 0.025346$	Heat flux:10^3–10^5 W m^{-2} Working fluid: water, Ethanol, and Acetone
26	Hazi and Markus [52]	$D_d \approx \sqrt{\frac{\sigma}{g(\rho_l-\rho_g)}}$	Focused on the effect of gravity acceleration
27	Unal [73]	$D_d = 2.42\times10^{-5}P^{0.709}\frac{a}{\sqrt{b\phi}}$ In which $a = \frac{\Delta T_{sat}k_f\gamma}{2\rho_g h_{fg}(\pi\alpha_f)^{1/2}}, b = \frac{\Delta T_{sub}}{2(1-\frac{\rho_g}{\rho_l})}$	Working fluids: Water, pressure: 0.1–17.7 MN m^{-2}; heat flux: 0.47–10.64 MN m^{-2}
28	Kocamustafaogullari and Ishii [51]	$D_d = 2.64\times10^{-5}\theta(\frac{\Delta\rho}{\rho_g})^{0.9}\sqrt{\frac{\sigma}{g\Delta\rho}}$	–
29	Basu et al. [50]	$D_d = l_c 1.3(\sin\theta_m)^{0.4}\left[0.13e^{-1.75\times10^{-4}\mathrm{Re}_l}+0.005\right]\times Ja_{sup}^{0.45}\exp(-0.0065Ja_{sub})$	Pressure: 1.03–3.2 bar, heat fluxes: 2.5 – 90 W m^{-2}
30	Bae [74]	$D_d = (1+8.34\left[\frac{C_{sl}}{\cos\theta_i}\left(\frac{D_d u_r}{A^2}\right)^2\right]^{-0.7})$	–

Additionally, Cho et al. [49] experimentally studied forces acting on a bubble for determining the bubble departure and lift-off from a heated surface. The proposed model for the departure diameter relies extremely on the contact angle. The comparison of different models associated with the bubble departure diameter is shown in Fig. 10. The departure diameter was overestimated by the correlations proposed by Basu [50] and Kocamustafaogullari [51].

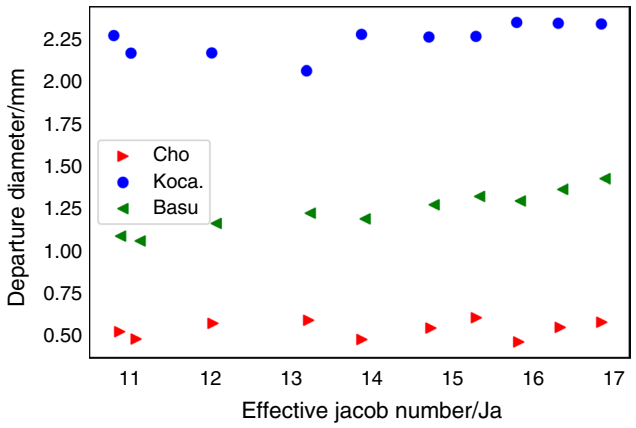

Fig. 10 Bubble departure diameter based on different correlations [49]

On the other hand, Hazi and Markus [52] numerically investigated bubble growth on a horizontal plate in slow-moving and stagnant fluid utilizing a lattice Boltzmann method. Using simulations, the bubble departure frequency and diameter were estimated, and specifically, in a stagnant fluid, they found that the departure diameter is proportional to $g^{-1/2}$, where g is the gravitational acceleration. Ardon et al. [53] introduced a model to predict bubble departure diameters and dynamic contact angles during pool boiling. According to their model, fluid drag forces have a significant effect on the bubble shape rather than surface tension

forces in the condition of high Jakob numbers ($Ja > 100$) and fast-growing bubbles, which leads to a hemispherical shape in the growth period. On the other hand, the condition of the slow-growing bubble with low Jakob numbers ($Ja < 50$) results in a spherical shape of the bubble.

According to the proposed correlations, it can be roughly mentioned that most of correlations for the bubble departure diameter have a general form,

$$D_d = A \cdot Ja^B \cdot \left(\frac{\sigma}{\rho_l - \rho_v} \right)^C \tag{39}$$

where A, B, and C are constant.

Active nucleation site density (n_s)

As aforementioned, bubble growth can be categorized into two nucleation processes, including homogeneous nucleation and heterogeneous nucleation [75]. The former describes the creation of bubbles at a vapor–liquid interface in superheated liquid without a heating surface, vapor nuclei, and pre-existing gas, while the latter expresses the creation of bubbles at a vapor–liquid interface with the existence of vapor or gas in a cavity on a heated surface [33]. In heterogeneous nucleation, cavities serve as nucleation sites, and the quantity of cavities is one of the important parameters of consideration in heat transfer. Not all the cavities generate bubbles and, therefore, a minimum cavity radius exists at a specific heat flux so that the cavities greater than the minimum radius can generate vapor bubbles, named as active nucleation sites. The active nucleation site density is referred as the cavities' number which can form a vapor bubble per a unit heating surface area.

The active nucleation site density coupled with the bubble departure diameter is closely correlated with the boiling heat flux or the boiling heat transfer coefficient. Many researchers have developed different correlations to determine the nucleation site density, as summarized in Table 2. For instance, the first correlations for the active nucleation site density were proposed by Gaertner and Westwater [76] and Micki and Rohsenow [77]. Gaertner and Westwater [76] performed an experiment associated with pool boiling on a horizontal flat copper surface by using an aqueous solution of nickel salts including 20% solids as a working fluid at atmospheric pressure. The applied ranges of the wall superheat and heat flux were from 8.1 to 102.67 °C and from 24.2 to 1687.7 kW m^{-2}, respectively. They observed that the nucleation site density and square of heat flux are proportional. On the other hand, Zou and Jones [78] experimentally

Table 2 Correlations of active nucleation site density proposed by different researchers

No	References	Correlations	Condition
1	Gaertner and Westwater [76]	$n_s \approx q^{2.1}$	Aqueous solution of nickel salts on copper surface at atmospheric pressure
2	Micki and Rohsenow [77]	$n_s \approx \left[D_{c,max}/D_c\right]^m$ $D_c = \frac{4\sigma T_{sat}}{\rho_v h_{lv}(T_w - T_{sat})}$, m = 6.5	–
3	Bier et al. [80]	$\ln n_s = \ln(n_{max})\left[1 - (\frac{D_c}{D_{c,max}})^m\right]$	Horizontal copper plates, Working fluid: boiling refrigerants Rll ($CFCl_3$) and Rll5(C_2F_5Cl)
4	Cornwell and Brown [81]	$n_s \approx (T_w - T_{sat})^{4.5}$	–
5	Paul and Abdel-Khalik [82]	$n_s = 1.027 \times 10^{-3} q + 15.74$	Water on an electrically heated platinum wire at atmospheric pressure
6	Kocamustafaogullari and Ishii [51]	$n_s^+ = f(\rho^+) R_c^{+(-4.4)}$ $n_s^+ = n_s D_d^2$, $f(\rho^+) = 2.157 \times 10^{-7} \rho^{+(-3.2)}(1 + 0.0049\rho^+)^{4.13}$ $\rho^+ \equiv \frac{(\rho_l - \rho_v)}{\rho_v} R_c^+ = \frac{2R_c}{D_d}$	–
7	Yang and Kim [83]	$n_s = \overline{n}_s \int_0^{\frac{\theta}{2}} \frac{1}{\sqrt{2\pi s}} \exp\left\{\frac{-(\beta - \overline{\beta})^2}{2s^2}\right\} d\beta \times \int_{R_c}^{R_s} \lambda \exp(-\lambda R_c) dR_c$	–
8	Wen and Wang [84]	$n_s = 5 \times 10^5 (1 - \cos\theta) D_c^{-6}$	Water at 1 atm pressure on Cu surfaces
9	Benjamin and Balakrishnan [85]	$n_s = 218.8(\mathrm{Pr})^{1.63}\left(\frac{1}{\gamma}\right)\sqrt{\frac{k_l \rho_l C_{pl}}{k_w \rho_w C_{pw}}}\phi^{-0.4}(T_w - T_{sat})^3$ $\gamma = \left(\frac{k_w \rho_w C_{pw}}{k_l \rho_l C_{pl}}\right)^{1/2}$, $\phi = 14.5 - 4.5(R_a P/\sigma) + 0.4(R_a P/\sigma)^2$	Distilled water, acetone, n- hexane, and carbon tetrachloride on aluminum and stainless steel surfaces
10	Sakashita and Kumada [86]	$n_s = C_s\left[(Ja \times R_c)^{3/10}(\frac{1}{R_c})\right]^m$	–

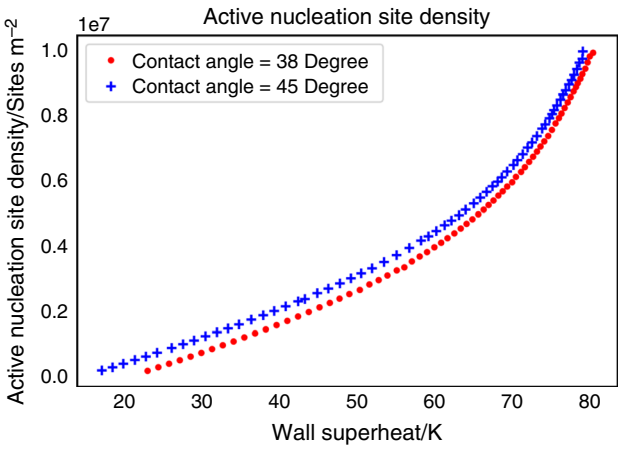

Fig. 11 Active nucleation site density with different wall superheats based on models developed by Habiki and Ishii [79]

studied nucleation site distributions on stainless steel and copper heating surfaces with subcooled boiling of R134a. To achieve reliable results, high-speed cameras were used for recording bubble images from the heated surfaces. According to their results, the nucleation distributions were fairly more uniform on the copper surface when compared with the stainless-steel surface. In another study, Habiki and Ishii [79] developed a model to estimate the active nucleation site density with various wall superheats in contact angles of 38° and 45° (Fig. 11). Based on the figure, the active nucleation site densities are augmented by increasing the wall superheat.

Bubble waiting period (t_w)

In addition to bubble departure diameter and active nucleation site density, bubble waiting period is another crucial parameter that influences the heat transfer rate from a heated surface through nucleate boiling [33]. A bubble waiting period is the time period between the bubble departure from a nucleating cavity and the subsequent bubble initiation from the same cavity. To determine this period, an equation relying on the bubble nucleation and potential flow theory principles has been introduced by Han and Griffth [43].

$$t_w = \frac{9}{4\pi\alpha_l}\left\{\frac{(T_w - T_\infty)R_c}{(T_w - T_s)\left[1 + (2\sigma/R_c\rho_v h_{lv}\right]}\right\}^2 \quad (40)$$

where σ and R_c are the surface tension and cavity radius, respectively. T_w, T_∞, and T_s are referred to the temperature of wall, bulk liquid, and the heated surface, respectively.

Basu et al. [50] correlated the bubble waiting period as a function of wall superheat:

$$t_w = 139.1\ (\Delta T_w^{-4.1}) \quad (41)$$

On the other hand, Philips et al. [8] determined that the bubble waiting period not only depends on the wall superheat, but also thermal diffusivity and liquid subcooling. Other researchers added more parameters in their correlations such as heat flux, properties of the heated surface, and bulk liquid velocity [9, 10]. Maity [11] concluded that the bubble waiting time is increased by increasing the bulk liquid velocity. Another correlation derived by Hsu and Graham [87] stated that the waiting period depends upon the thermal boundary layer thickness and the bulk temperature of the fluid. Hsu and Graham [87] also developed the minimum waiting period with making the bubble equilibrium temperature curve and the fluid temperature line tangent to each other like:

$$t_{w,min} = \frac{144(T_w - T_\infty)T_s^2\sigma^2}{\pi\alpha_{lv}\rho_v^2 h_{lv}^2(T_w - T_s)^4} \quad (42)$$

An expression for the bubble waiting period (t_w) and bubble growth period (t_g) for pure liquids has been developed by Van Stralen et al. [11] as follows:

$$t_w = 3t_g \quad (43)$$

In accordance with the equation of bubble waiting period and bubble growth period, the former is three times greater than the latter in the equal nucleation cavity.

Bubble growth rate ($R(t)$)

Another significant parameter contributing to the bubble dynamics parameters is the bubble growth rate, defined as the modification in bubble size over time [33]. Table 3 summarizes various bubble growth models throughout nucleate boiling under several conditions such as uniform and non-uniform temperature fields and different pressures. In the correlation introduced by [35, 39], the square root of time, thermal diffusivity, and Jakob number affect bubble growth rate. It can be observed that this fact is valid for most of the correlations. Cole and Shulman [42] used ¾ power of the Jakob number, while Labuntsov et al. [88] proposed square root of the Jakob number in their bubble growth model. The table shows that different coefficients have been suggested in different correlations [89–92]. Moreover, the Prandtl number, the growth period, and the bubble waiting period have been involved in the models of the bubble growth rate introduced by Copper [93], Van Stralen and Sluyter [89], and Mikic et al. [9], respectively.

The analytical models proposed by Plesset and Zwick [35] and Zuber and Foster [38] were formulated based on the heat diffusion from a superheated layer surrounding the

Table 3 Correlations of the bubble growth rate proposed by different researchers

No	Reference	Correlations	Condition
1	Firtz and Ende [90]	$R(t) = 1.128Ja\sqrt{\alpha_l t}$	–
2	Van Stralen and Sluyter [89]	$R(t) = 1.954b\left[\exp\left(\frac{t}{t_g}\right)\right]^{0.5} Ja\sqrt{\alpha_l t}$ b = constant bubble growth parameter for spherical bubble $b \leq 0.794$	Pure liquids and binary mixtures
3	Plesset and Zwick [35]	$R(t) = \left(\frac{12}{\pi}\right)^{1/2} Ja(\alpha t)^{1/2}$ at uniform temperature field	–
4	Forster and Zuber [38]	$R(t) = \sqrt{\pi} \times Ja(\alpha t)^{1/2}$ at uniform temperature field	–
5	Zuber [39]	$R(t) = \frac{2b}{\sqrt{\pi}} \times Ja(\alpha t)^{1/2}$ Uniform temperature field $R(t) = \frac{2b}{\sqrt{\pi}} \times Ja(\alpha t)^{1/2}\left[1 - \frac{q_b\sqrt{\pi\alpha t}}{2k\Delta T}\right]$ Non-uniform temperature field	–
6	Labunstov et al. [88]	$R(t) = \sqrt{2\beta.Ja}(\alpha t)^{1/2}$ Pressure: 1–100 bar $\beta = 2\cos(\theta/2)\ln\frac{\Delta}{y_A}\left[(1+\cos\theta)^2(2-\cos\theta)\right]^{-1}$	Working fluid: water
7	Cole and Shulman [42]	$R(t) = \frac{5}{2}Ja^{3/4}(\alpha t)^{1/2}$ High Jakob number	–
8	Cooper [93]	$R(t) = 2.5\frac{Ja}{\mathrm{Pr}_l^{0.5}}(\alpha t)^{1/2}$	Water, organic liquids, cryogens and metallic fluids have been used
9	Mikic et al. [9]	$R^+ = \frac{2}{3}\left[(t^+ + 1)^{3/2} - (t^+)^{3/2} - 1\right]$ $R^+ = \frac{R}{B^2/A}, t^+ = \frac{t}{B^2/A^2}$ $A = \left[b\frac{\Delta T h_{fg}\rho_v}{T_{sat}\rho_l}\right]^{1/2}, B = \left[\frac{12}{\pi}Ja^2\alpha_l\right]^{1/2}$	–
10	Akiyama [91]	$R(t) = Ja^{3/5}\alpha^{1/2}t^n$ Jakob number: 2–1040	Working fluids: water, ethanol, and carbon-tetra-chloride
11	Chen et al. [92]	$R^* = Kt^{*n}$, Pressure: 1–10 bar $R^* = \frac{R}{(La/2)}, La = \left[\frac{\sigma}{(\rho_l-\rho_v)g}\right]^{1/2}, t^* = \frac{t}{\xi}$	Working fluid: DI water, Pressure: 1–10 bar,
12	Zhao et al. [94]	$R(t) = \frac{2k(T_w - T_{sat})}{\rho_l h_{lv}\sqrt{0.64\,\mathrm{Pr}\,\alpha_l}}\sqrt{t}$	–
13	Yun et al. [95]	$R(t) = \frac{2b}{\sqrt{\pi}}Ja\sqrt{\alpha t} - \frac{bq_b t}{sh_{lv}\rho_v}$, $B = 1, s = 2$	–
14	van Stralen et al.[11]	$R(t) = 0.47 \times Ja \times \mathrm{Pr}^{\frac{-1}{6}}\sqrt{\alpha t}$	–

bubble. In addition to heat diffusion from the superheated layer, Yun et al. [95] incorporated the effect of condensation at the bubble cap for calculating bubble growth rate. Cooper and Lloyd [93] and van Stralen et al. [11] proposed the bubble growth rate model considering an evaporation layer as the major source of heat addition to the bubble. From the formulations presented in Table 3, it can be seen that the bubble growth rate due to heat transfer from evaporative and relaxation layers is proportional to $t^{1/2}$. Different model constants are used to take care of different amounts of heat transfer from each layer. Roughly, the general form of the bubble growth R(t) at any time t in terms of constant A and B can be provided as follows:

$$R(t) = A\left[Ja \times (\alpha t)^{0.5}\right] - B\left[\frac{q'' t}{h_{lv}\rho_v}\right] \tag{44}$$

The first term in the above expression accounts for the heat transfer contribution either from the evaporative layer, the superheated layer or from both. The second term represents the effect of condensation from the bubble dome in contact with subcooled liquid.

Bubble growth period (t_g)

Bubble growth period is the time interval from the initiation of a vapor bubble in a cavity until it departures from the cavity, and it significantly influences the magnitude of heat removed from a heated surface[33]. A correlation for the bubble growth period in non-uniform temperature fields in the liquid has been proposed by Zuber [39] and this correlation is a function of the thermal diffusivity of the liquid phase, bubble departure diameter, and Jakob number (Ja), expressed as

$$t_g = \frac{D_d^2}{16b^2(Ja)^2\alpha_l} \tag{45}$$

where b is a constant ranging from 1 to $\sqrt{3}$. It should be noted that the bubble growth period is proportional to the square of the bubble departure diameter. Another correlation for bubble growth period has been proposed by Hatton and Hall [56] by utilizing the Plesset and Zwick's [35] bubble growth period relation and Zuber's parameters [39] with the cavity radius and without the Jakob number.

$$t_g = \frac{\pi\alpha_l}{3}\left\{\frac{\left(\rho_v h_{lv}\right)^2 D_d R_c}{8k_l\sigma T_{sat}}\right\}^2 \tag{46}$$

The equation shows that the bubble growth period depends on the square of the nucleation cavity radius and a bubble departure diameter. Besides, the dimensionless bubble growth period has been investigated by Lee et al. [65], which is roughly 60 for constant wall temperature and R11 and R113 working fluid at saturated boiling conditions. They proposed a correlation of bubble growth period with applying this dimensionless growth period.

$$t_g = 67.5Ja\alpha\rho_l\frac{D_d}{\sigma} \tag{47}$$

According to this correlation, the bubble growth period is changed with the bubble departure diameter and Jakob number with respect to surface temperature.

Bubble departure frequency (f)

Another essential parameter affecting the bubble dynamics used for determining the boiling heat transfer coefficient is the bubble departure frequency [33]. The bubble departure frequency is a strong function of the bubble growth period (t_g) and the bubble waiting period (t_w). It is the reciprocal of the time interval contributed to two subsequent nucleations within nucleate boiling. In experiments, the bubble departure frequency can be measured by counting the overall number of bubbles generating from a cavity per unit recording time and can be expressed as

$$f = \frac{1}{(t_w + t_g)} \tag{48}$$

Based on the correlations for t_w and t_g, the wall superheat, interactions between adjacent bubbles, cavity size, phase contact angle, and thermophysical properties of fluid have significant effects on the bubble departure frequency.

Jakob and Linke [96] are pioneers who defined a correlation of the bubble departure frequency with respect to the bubble waiting period, bubble velocity, bubble growth period, and bubble departure diameter. A few years later, Jakob and Fritz [97] found that the product of the bubble departure diameter and departure frequency is constant during pool boiling of liquid nitrogen and water. In another study, Jakob [97] adjusted the product of the bubble departure diameter and departure frequency by considering the thermophysical properties of the working fluid and surface tension. In his study, it was assumed that the bubble waiting period and the growth period are equivalent. Later, Jakob's correlation was modified by Peebles and Garber [98] and McFadden and Grassman [99]. In particular, McFadden and Grassman's study found that the product of a square root of bubble departure diameter and bubble departure frequency ($fD_d^{0.5}$) is constant. Zuber [100] also proposed a modified Jakob's correlation [101] by considering the equivalence of the bubble growth period and waiting period.

Additionally, Hatton and Hall [56] proposed a correlation that shows the dependency of the square of the bubble departure diameter and bubble departure frequency on the liquid thermal diffusivity. Also, Cole [10] introduced an expression between departure frequency and bubble departure diameter respect to the gravity and density ratio under buoyancy and drag forces. However, in accordance with the experimental data, the values of surface tension and the power of bubble departure diameter are substituted by 4/3 and 0.5, respectively. Table 4 provides various correlations for bubble departure frequency.

Factors affecting the bubble dynamics parameters

Numerous factors govern bubble dynamics parameters associated with the boiling heat transfer. These factors can be categorized into two fundamental groups, namely active and passive. Active factors include electric and magnetic fields, ultrasonic waves, and vibration, while passive factors include heat flux, thermo-physical properties, contact angles, wall superheat, liquid subcooling, cavity spacing, gravity levels, surface roughness, and pressure [110, 111].

Table 4 Correlations of bubble departure frequency

No	References	Correlations	Condition
1	Jakob and Linke [102]	$fD_d = V_b\left[\frac{t_g}{(t_g+t_w)}\right]$	–
2	Jakob and Fritz [97]	$fD_d = 0.078$	–
3	Jakob [101]	$fD_d = \left[\frac{\sigma g(\rho_l-\rho_v)}{\rho_l^2}\right]^{1/4}$	–
4	Peebles and Garber [98]	$fD_d = 1.18\left[\frac{t_g}{(t_g+t_w)}\right]\left[\frac{\sigma g(\rho_l-\rho_v)}{\rho_l^2}\right]^{1/4}$	–
5	McFadden and Grassman [99]	$fD_d^{0.5} = 1.75$	Working fluid: liquid nitrogen
6	Zuber [100]	$fD_d = \left(\frac{1.18}{2}\right)\left[\frac{\sigma g(\rho_l-\rho_v)}{\rho_l^2}\right]^{1/4}$	–
7	Hatton and Hall [56]	$fD_d^2 = 284.7\alpha_l$	Boiling on stainless steel rod
8	Cole [10]	$fD_d^{0.5} = \left[\frac{4g(\rho_l-\rho_v)}{3\rho_l}\right]^{1/2}$	Pressure: 50–760 mm Hg
9	Ivey [103]	$fD_d^{0.5} = 0.9g^{1/2}$ $fD_d^{3/4} = 0.44g^{1/4}$	–
10	Mikic and Rohsenow [9]	$f^{\frac{1}{2}}D_d = \left(\frac{4}{\pi}\right)Ja\sqrt{3\pi\alpha_l}\left[\left(\frac{t_g}{t_g+t_w}\right)^{\frac{1}{2}} + \left(1+\frac{t_g}{t_g+t_w}\right)^{\frac{1}{2}} - 1\right]$	The relation is valid in both regions: inertia controlled and heat diffusion-controlled growth
11	Malenkov [104]	$fD_d = \frac{v_b}{\pi}\left(1-\frac{q}{v_b\rho_v h_{lv}}\right)$ $v_b = \left[\frac{D_d g(\rho_l-\rho_v)}{2(\rho_l+\rho_v)} + \frac{2\sigma}{D_d(\rho_l+\rho_v)}\right]^{\frac{1}{2}}$	–
12	Katto and Yokoya [105]	$f = \left(\frac{3\lambda_T^2 q}{4\pi\rho_l h_{lv}}\right)^{-1/5}\left[\frac{4(\xi\rho_l-\rho_v)}{g(\rho_l-\rho_v)}\right]^{-3/5}$ $\lambda_T = 2\pi\left[\frac{3\sigma}{\rho_l-\rho_v}\right]^{0.5}, \xi = 11/16$	–
13	Stephan [106]	$fD_d = \frac{1}{\pi}\left[\frac{g}{2}\left(D_d + \frac{4\sigma}{\rho_l g D_d}\right)\right]^{\frac{1}{2}}$	–
14	Kumada and Sakashita [107]	$f = 0.215\frac{\left[\frac{g(\rho_l-\rho_v)}{\rho_l}\right]^{\frac{5}{9}}}{(v_l D_s^3)^{\frac{1}{9}}}$	Working fluids: water, ethanol and Freon-113 at high heat fluxes and atmospheric pressure
15	Sakashita and Ono [108]	$f = 0.6\left[\frac{g(\rho_l-\rho_v)}{\rho_l}\right]^{\frac{2}{3}}\left\{v_l\left[\frac{g(\rho_l-\rho_v)\rho_l^2 v_l^4}{\sigma^3}\right]^{-0.25}\right\}^{-1/3}$	Working fluid: water, Surface: a horizontal, upward-facing plate Pressure: 1 atm to 7 MPa,
16	Miglani et al. [109]	$f^+ = 28.89Bo_m + 116.8$ $Bo_m = \frac{q}{Gh_{lv}}, G = \frac{\pi}{6}D_d^3\rho_v f n_s$	Working fluid: R-134a
17	Hamzekhani et al. [90]	$f = 0.015\left(\frac{\Delta\rho^{0.25}g^{0.75}}{\sigma^{0.25}}\right)\left(\frac{q}{\Delta\rho^{0.25}g^{0.75}\sigma^{0.75}}\right)^{0.44}\left(\frac{\Delta\rho^{0.25}g^{0.75}D_d}{\sigma^{0.5}}\right)^{0.88}$	Working fluids: water and water/NaCl at atmospheric pressure

All the mentioned factors are shown in Fig. 12. This section focuses on a detailed review on the influence of these active and passive factors on bubble dynamics parameters to better predict the boiling heat flux or heat transfer coefficient.

External electric field

The first influential factor in bubble dynamics parameters and boiling heat transfer is an external electric field in the working fluid inducing an electrohydrodynamic (EHD) effect [112–114]. Chubb [112] is a pioneer who applied an external electric field to improve boiling heat transfer. Thereafter, several studies have been carried out into applications of the EHD effect on studying the bubble dynamics parameters and boiling heat transfer. Table 5 summarizes some of these studies with their main findings. It can be observed from the table that the EHD effect plays different roles in their studies because different researchers used various configurations and arrangements of the electrodes.

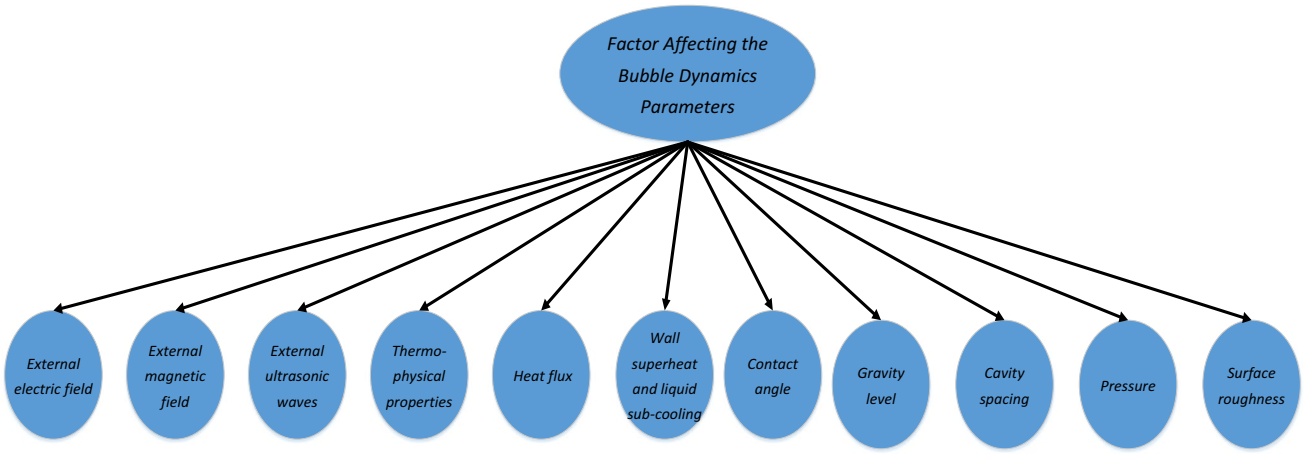

Fig. 12 Various factors affecting the bubble dynamics parameters

Table 5 Effects of an external electric field on the bubble dynamics parameters

Researcher	Working fluid	Electrode/heater geometry	Number of bubbles	Growth period	Waiting period	Departure frequency	Departure diameter	Suppressed bubble?	Enhanced boiling heat transfer
Ogata and Yabe [115]	R113(R11) + Ethanol	Mesh electrode, large heating surface	Increase	NA	NA	Increase	Decrease	Yes	Yes
Karayiannis and Xu [116]	R-123	Rod electrode, tube bundles	Increase	NA	NA	NA	NA	Yes	Yes
Kwen and Kim [118]	R-113	Plate electrode, heating wire	Increase	Decrease	Decrease	Increase	Decrease	No	Yes
Pascual et al.[119]	R-123	Mesh electrode, platinum heating wire	Not increase	NA	NA	NA	Decrease	NA	NA
Madadnia and Koosha [117]	R123	Wire electrode, heating wire	Not increase	Increase	NA	Increase	Increase	Yes	Yes
Siedel et al. [120]	n-Pentane	Mesh electrode, copper cylinder	Single bubble	NA	NA	NA	Increase	No	Yes
Chen et al. [121]	R-113	Mesh electrode, brass block	Single bubble	Increase	Decrease	Increase	Decrease	No	NA
Gao et al. [112]	R-113	Needle electrode, small heating surface	Single bubble	Increase	Increase	Decrease	Decrease	Yes	Yes

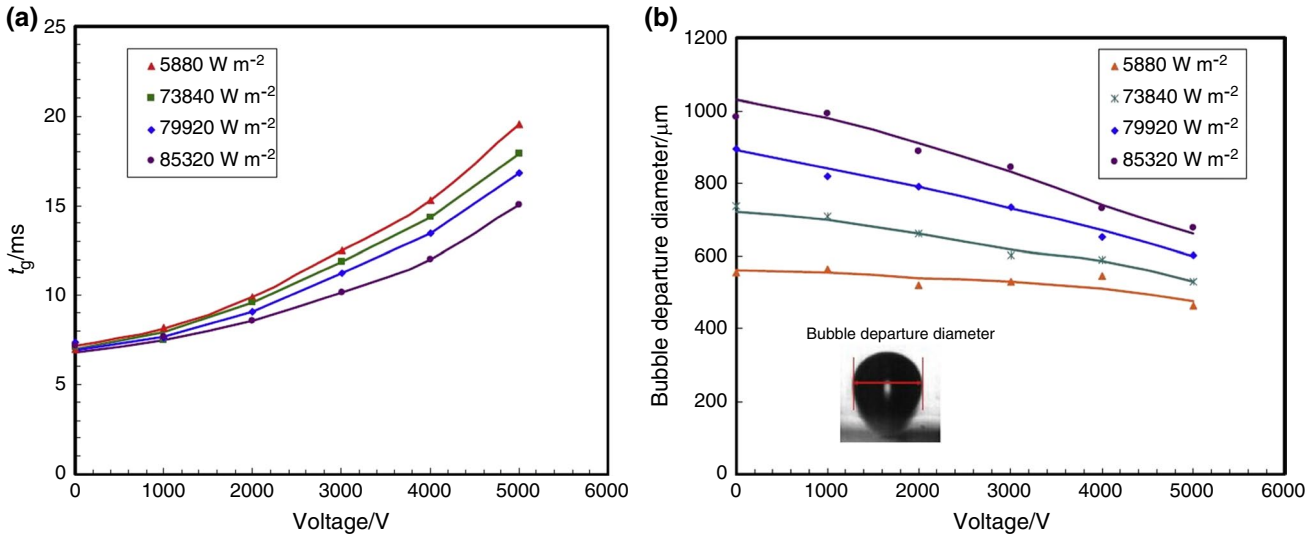

Fig. 13 Effect of the electric field on a) the bubble growth rate and b) bubble departure diameter with various heat fluxes. [112]

For instance, Ogata and Yabe [115] utilized an electric field in their experiment in phase-change fluids. The number of boiling bubbles and the bubble departure frequency was increased, and the bubble departure diameter was reduced once an external electric field was applied. Additionally, the boiling heat transfer of R-123 was experimented by Karayiannis and Xu [116] using rod electrodes at a high DC voltage of 20 kV. The results showed boiling heat transfer was enhanced more than 4.9 times. Madadnia and Koosha [117] used a wire electrode and a heating wire to determine the effects of EHD. According to the study, the EHD effects on bubble frequency and diameter became evident once heat flux and electric voltage exceeded 6 kW/m^2 and 6 kV, respectively. All these studies, including some others [116–119], the boiling experiments have been performed with a number of bubbles generated from a large heated surface, and therefore, statistical methods must be adapted.

Recently, Siedel et al. [120] and Chen et al. [121] studied the effects of a quasi-uniform electric field on a single bubble generation from an artificial nucleation site. The growth, departure, and rise of a single bubble with and without an electric field were studied. They found that the bubble diameter and boiling heat transfer were increased by introducing the electric field. Contrarily, the departure frequency and growth rate were not changed considerably. Figure 13 shows the effect of the electric field on the bubble growth rate and departure diameter with various heat fluxes. As it can be observed in the figures, the bubble growth rate increases by applying external electric field and this increase is obtained by augmenting the external voltage. Also, Chen et al. [121] concluded that the bubble departure diameter and growth rate were increased, while the bubble waiting time was reduced.

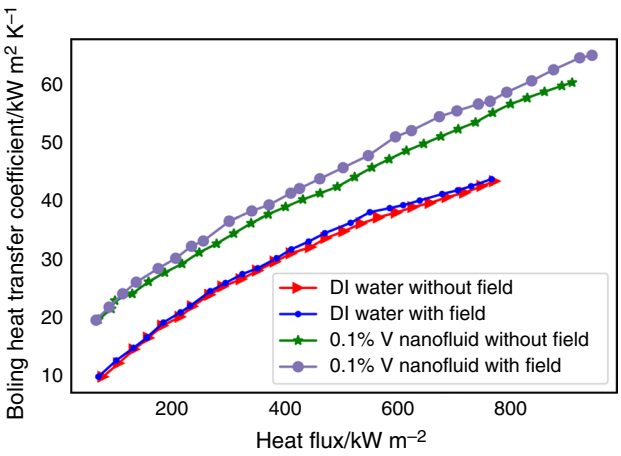

Fig. 14 The boiling heat transfer coefficient with respect to heat flux for 0.1% volume concentration nanofluid and base fluid with the negative magnetic field gradient (the gradient of the magnetic field decreases from bottom to the top of the boiling chamber) [124]

External magnetic field

An external magnetic field is another factor controlling the bubble dynamic parameters and the boiling heat transfer rate, and this field can be generally used once a working fluid has magnetic particles like Fe_2O_3. There are few studies about the effect of the magnetic field on the bubble dynamics parameters and nucleate boiling [122], and we found contradictory results of the changes in the bubble diameter under the magnetic fields. For instance, Liu et al. [123] investigated the nucleate boiling of Fe_3O_4/water nanofluid on a vertical heated bar by applying a non-uniform magnetic field. They found that the non-uniform magnetic field induced a

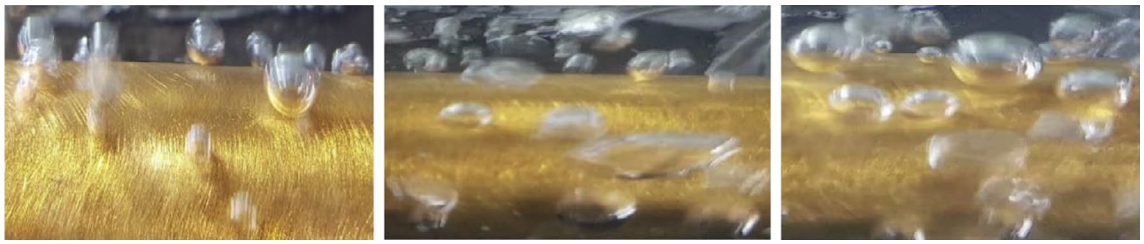

Fig. 15 Effect of ultrasonic power on the bubble departure diameter[125]

decrease in the nominal bubble departure diameter. However, the magnetic field changes the bubble shape greatly, eventually leading to an enhancement of the boiling heat transfer. In their study, the bubble shape was significantly distorted from the hemispherical structure under the magnetic field; it had a wider surface area at the bottom on the heated surface and became slender toward the top. The wider surface area of the bubble's bottom increased the region of the extreme temperature gradient, resulting in active microlayer evaporation and, therefore, faster bubble growth and higher bubble departure frequency.

On the other hand, some studies have shown a conflicting effect of the magnetic field on the bubble dynamics parameters. Abdollahi et al. [124] performed an experimental analysis using Fe_3O_4/water nanofluid with the presence of the magnetic field during pool boiling. They found that the magnetic force applied toward the heated surface caused the bubble to be pulled horizontally such that the bubble was stretched from the center in a higher magnetic field to the sides in the lower magnetic field. This change of the bubble shape results in an increase in the bubble diameter in the horizontal direction. The increase in bubble diameter with the magnetic field leads to an increase in the boiling heat transfer coefficient, as shown in Fig. 14.

Ultrasonic waves

External ultrasonic waves applied through a liquid is another influencing factor on the bubble dynamics parameters and nucleate boiling. A few studies have been carried out to evaluate the role of ultrasonic waves on the bubble dynamics parameters and boiling heat transfer. Kooshechin et al. [125] performed experiments with surfactants and nanofluids. The ultrasonic waves increased the bubble departure diameter and induced a more significant mixing and turbulence in the boiling solution, finally leading to a higher heat transfer coefficient. Some example figures of their study are shown in Fig. 15. As shown in the figure, the bubble diameter increases considerably by increasing the ultrasonic power from 30 to 60%. They found that more vibrant bubble movements were observed in all directions by increasing ultrasonic power.

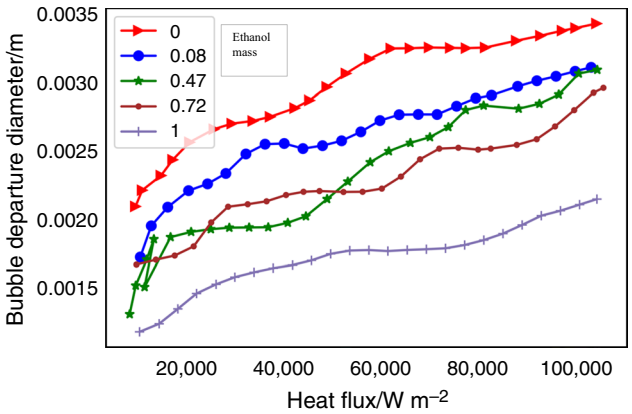

Fig. 16 Bubble departure diameter of water/ethanol solutions with respect to heat flux [127]

Thermophysical properties of fluid

Thermophysical properties of fluid significantly affect the correlations of bubble dynamics parameters, particularly for bubble departure frequency, bubble waiting period, bubble growth period, and bubble departure diameter. As an example, Gong et al. [126] found in their experiments that the smaller bubble departure frequency and lager bubble departure diameter were observed in pure ethane when compared with pure isobutene during pool boiling. They also found that the bubble departure frequency and diameter were changed considerably in the binary mixture of ethane and isobutene when the concentration increased. Lamas et al. [70] studied the bubble departure diameter of water, R134a, and R-123 and found that the diameter were different due to the modification in surface tension. In addition to the surface tension, the changes in interfacial tension were proven to modify the bubble dynamics parameters in many studies. Hamzekhani et al. [71] observed a smaller bubble departure diameter in ethanol when compared to water

Table 6 Summary of the effect of nanofluids in nucleate boiling

Reference	Type of nanofluid	Heat transfer enhancement/%
Cieliski et al. [134]	Al_2O_3-water	171
Truong [135]	Al_2O_3-water	56
Muhammad Ali et al. [136]	TiO_2-water	222
Milanova and Kumar [137]	SiO_2-water	150–200
Rainho et al. [138]	Fe_2O_3-water	129
Bang et al. [139]	Al_2O_3-water	32
You et al. [140]	Al_2O_3-water	200
Kim et al. [141]	TiO_2-water	180
Kim and Bang [142]	SiO_2-water	80
Kim and Bang [142]	ZrO_2-water	72
Padhye et al. [143]	Graphene oxide–water	179
Padhye et al. [143]	Graphene-water	84
Hinswankar et al. [144]	ZnO-water	70–80
Kathiravan et al. [145]	Cu-water	25–50

because of the low interfacial tension between the surface and liquid. Additionally, Hamzekhani et al. [90] obtained a decrease and an increase in the bubble departure frequency and bubble departure diameter, respectively, by increasing the mass fraction of a NaCl solution. A larger bubble departure diameter has been observed in NaCl solution when compared to water because of the high interfacial tension in NaCl solution.

Gao et al. [127] performed an experiment to compare nucleate boiling characteristics of distilled water and calcium chloride aqueous solutions at sub-atmospheric pressure. They found that increasing the concentration of calcium chloride in the water led to a decrease in the bubble departure diameter and an increase in the bubble departure frequency. Hamzekhani et al. [71] performed experiments to measure the bubble departure diameter of pure water, ethanol, and different mixtures containing Na_2SO_4/water, ethanol/water, and NaCl/water. As depicted in Fig. 16, the bubble diameter augments by increasing the heat flux for all working fluids. In addition, some research has been done to understand the effects of modifying thermophysical properties of fluids on changing the bubble dynamics parameters. Fazel and Shafaee [68] performed experiments to measure the bubble departure diameter of NaCl, Na_2SO_4, and KNO_3 solutions and found that among these three solutions, the largest and smallest bubble departure diameters belong to NaCl and Na_sSO_4, respectively. Bovard et al. [72] observed that the range of bubble departure diameter for methanol and acetone is between water and ethanol with the modification of thermophysical properties of the fluid, affecting the vapor bubble growth. Moreover, various studies have been carried out to understand the effect of nanofluid as a working fluid in the nucleate boiling [19, 21, 128–130]. These studies used CuO-water [20, 129], graphene oxide–water (GO-water) [19], zirconia–water [21], Al_2O_3-water [131], TiO_2-water [132], and glycol–water alumina [130] nanofluids as the working fluid in pool boiling. Goodarzi et al. [19] used GO/H_2O nanofluid with different mass fractions on a small copper disk to measure the boiling heat transfer coefficient. They found that the presence of the nanoparticles decreased the boiling heat transfer coefficient due to the creation of a surficial fouling layer on the surface. Wang et al. [133] experimentally studied a single bubble growth and departure from a heated surface in nanofluid containing silica nanoparticles with different mass concentration (0.15%, 0.1%, and 0.05%). The results showed that the bubble departure frequency increased by augmenting the concentration of nanoparticles. However, the bubble departure diameter was not influenced considerably by the presence of the nanoparticles. Table 6 provides a summary of the effects of nanofluids in the nucleate boiling.

Table 7 Effect of heat flux on the bubble dynamics parameters

Reference	Working fluid	Bubble departure diameter	Bubble departure frequency	Bubble waiting period	Bubble growth rate	Active nucleation site density
Gong et al. [126]	Ethane, isobutene, and mixture	Increase	Increase	NA	NA	NA
Benjamin and Balakrishnan [85]	Distilled water, carbon tetrachloride, n-hexane, and acetone	NA	NA	NA	NA	Increase
Tong et al. [147]	Novec 7100	Increase	Increase	NA	NA	Increase
McHale and Garimella [152]	FC-77	Increase	Increase	NA	NA	Increase
Chien et al. [151]	Water	Decrease	Increase	Decrease	NA	Increase
Judd and Hwang [149]	Methylene chloride	Decrease	Increase	NA	NA	Increase
Nakayama et al. [150]	R-11/water	Decrease	Increase	NA	NA	NA

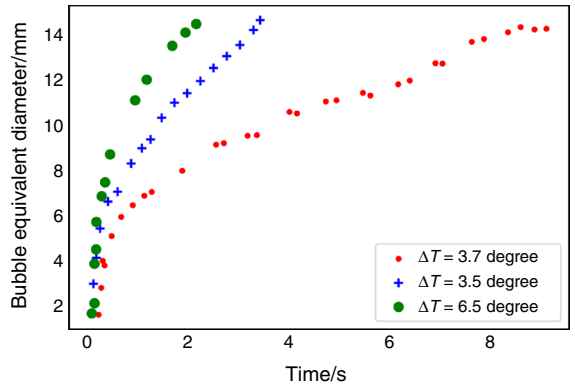

Fig. 17 Bubble diameter with respect to time at different wall superheats[155]

Heat flux

Bubble departure frequency, bubble departure diameter, and active nucleation site densities generally increase by increasing the heat flux. Numerous studies investigated the effect of the heat flux on the departure diameter using various fluids [66, 68, 71, 72, 126, 146, 147]. For instance, Gong et al. [126] studied the nucleate boiling heat transfer characteristics of ethane, isobutene, and their binary mixture. They found that the trend of departure diameter and frequency in terms of heat flux for binary mixture is increasing. Moreover, the identical augmented trend was observed associated with active nucleation site density and departure frequency [146, 147]. Wang and Dhir [84] and Benjamin and Balakrishnan [85] reported that the active nucleation site density is augmented by raising the heat flux. Gong and Cheng [148] verified that the bubble waiting period decreases by increasing the heat flux. The bubble departure frequency and the bubble departure diameter increases and decreases, respectively, by increasing the heat flux [149, 150]. Chien et al. [151] found that the bubble departure diameter and bubble growth period were reduced by increasing the heat flux, while the nucleation site density and bubble frequency were increased. Table 7 shows a summary of various studies for the effect of heat flux on the bubble dynamics parameters.

Wall superheat and liquid subcooling

Wall superheat influences the bubble dynamics parameters, as shown by some researchers. McHale and Garimella [152] experimentally investigated the impact of increasing wall superheat and concluded that the nucleation site density,

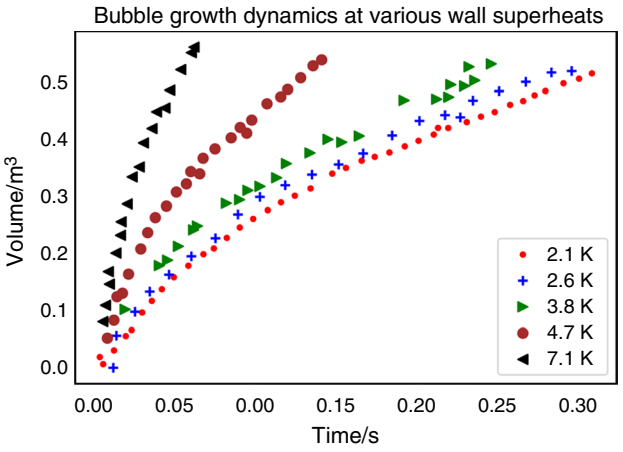

Fig. 19 Bubble volume with respect to time in different wall superheats (data extracted from Siedel et al. [156])

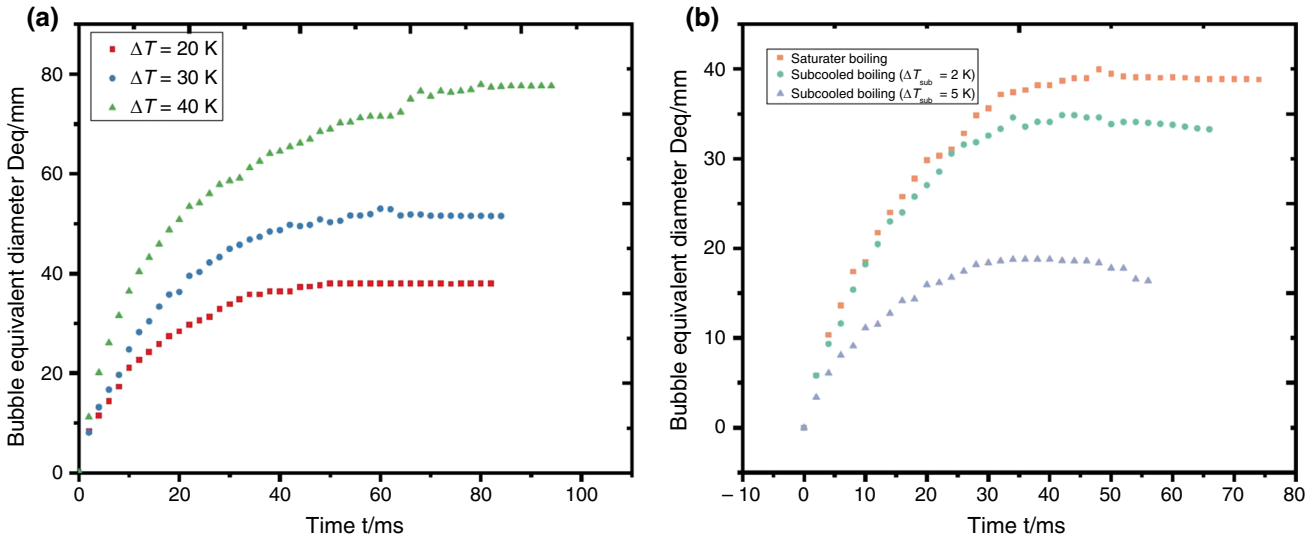

Fig. 18 Bubble diameter of distilled water at different superheat temperatures **a** at $P = 5.6$ kPa and **b** at $P = 20$ kPa) measured by Gao et al. [127]

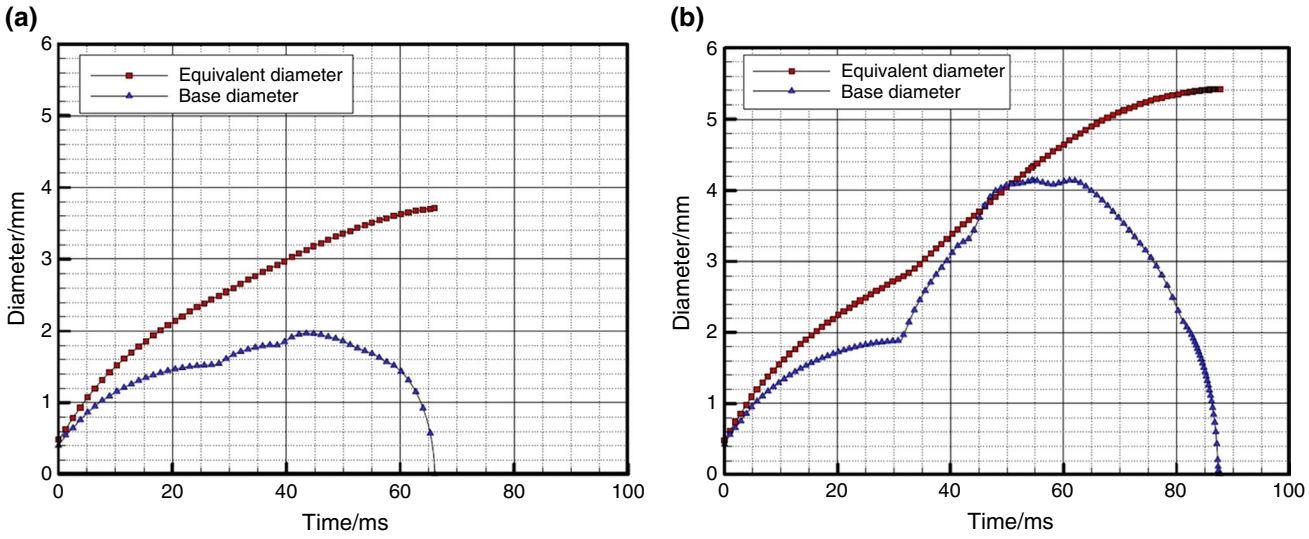

Fig. 20 Bubble growth **a** receding contact angle 48°, advancing 61°, **b** receding contact angle 54°, advancing 90° [159]

bubble departure frequency, and bubble departure diameter increase during pool boiling of perfluorinated hydrocarbon (FC-77) on rough and smooth surfaces with roughness amount (Ra) of 0.03 and 5.89 µm. Gong and Cheng [148] obtained similar outcomes associated with the bubble departure diameter whereas the bubble growth period reduces by augmenting wall superheat. Additionally, Zuber [153] reported that the bubble departure diameter rises by increasing the wall superheat due to a thicker superheated thermal boundary layer. Furthermore, Dhir et al. [154] numerically studied the bubble growth rate and bubble departure diameter in which the results are in a good agreement with the experimental data of Qiu et al. [155]. As indicated in their results, the bubble departure diameter and growth rate increase with a rise in the wall superheat, whereas the growth period reduces. Moreover, the growth period and bubble departure diameter increase and decrease, respectively, with increasing the subcooling. The time-dependent bubble diameter at different wall superheats is shown in Fig. 17. As it is clear, the bubble diameter is increased, and the required time to create a bubble is decreased by augmenting the wall superheat. Siedel et al. [156] provided the same results in their experiments on a heated surface with artificial nucleation sites. In their study, bubble growth with different wall superheat has been measured (Fig. 18). Figure 19 shows the bubble growth with respect to time in different wall superheats. According to the results, by raising the wall superheat, the bubble growth time is considerably reduced.

Table 8 Experimental data regarding the effect of contact angle on a bubble departure diameter

Fluid	Operating pressure/$\times 10^5$Pa	Contact angle/°	Bubble departure diameter/$\times 10^{-3}$m
Water [161]	1	22	1.65
		31	1.48
		67	1.32
		80	0.99
		85	0.82
Water [47]	1	43	0.75
	1.93	45	0.78
	2.76	47	0.82
Water [162]	1	35	1.9
HFE-7100 [163]	1	25	1.1
R11 [65]	1	31	0.7
R113 [65]	1	11	0.8

Contact angle

The angle created by a liquid at the three-phase boundary in which solid, gas, and liquid meet so that provides the numerical measurement of wetting of a solid by liquid is named contact angle. The contact angle is split into two kinds, namely, static and dynamic contact angles, based on the three-phase boundary's movement. The dynamic contact angle can be calculated while the three-phase boundary is moving. These angels are named advancing and receding contact angles (maximum and minimum value of static contact angle). To evaluate the effect of contact angle on the bubble growth, the influences on a bubble's departure and growth on a horizontal heated surface in the period of

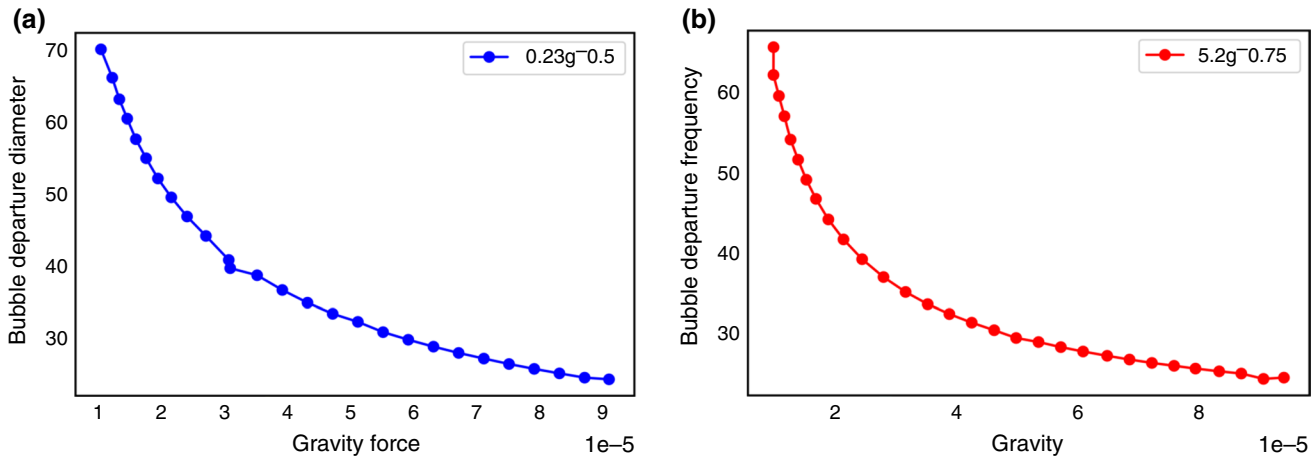

Fig. 21 (**a**) Bubble departure diameter as a function of gravity and (**b**) Bubble departure frequency as a function of gravity [52]

water and PF5060 pool boiling under normal gravity have been examined by Abarajith and Dhir [157]. Based on their results, the departure diameter of PF5060 becomes smaller with a contact angle of 10°, whereas the water's diameter with a contact angle of 35° becomes larger. Additionally, Mukherjee and Dhir's numerical model [158] was applied by Mukherjee and Kandlikar [159] for simulating an individual vapor bubble growth on a heated wall during nucleate boiling with a dynamic contact angle. The bubble initially grows with a spherical shape but gradually turns into a hemispherical shape due to the effect of the high advancing contact angle. The trend of bubble growth with different contact angles is shown in Fig. 20.

Also, Adron et al. [48] modeled the dynamic contact angles during pool boiling with various pressures, working fluids, and liquid superheats. In their results, the contact angle has a considerable effect on bubble departure diameter at high pressures. According to the model, fluid drag forces have a significant effect on the bubble shape rather than the surface tension force at high Jakob numbers (higher than 100) and fast-growing bubbles, which leads to a hemispherical shape in the growth period. On the other hand, the slow-growing bubble at low Jakob numbers (lower than 50) results in a spherical shape.

Furthermore, Phan et al. [160] presented a model predicting the relationship between contact angle and bubble departure on a horizontal surface. In their results, it was concluded that a function $tan\theta^{-1/6}$ describes the relationship between the bubble departure and contact angle. Table 8 shows some experimental studies regarding the effect of contact angle on the bubble departure diameter.

Gravity level

Another influential factor on the bubble dynamics parameters is the gravity level. Dhir et al. [154] numerically studied the bubble departure diameter and the growth period with respect to different gravity levels ($\frac{g}{g_e}$, g = gravitational acceleration, g_e = earth normal gravity) for water with a contact

Table 9 The effects of cavity spacing on the bubble behavior in the nucleate boiling

Reference	Working fluid	Surface properties	Cavity properties	Bubble behavior
Zhang and Shoji [165]	Distilled water	Thin silicon artificial surface	Two cylindrical cavities	The bubble departure frequency rises by varying this ratio between 1.5 to 2 and decreases while $\frac{S}{D_d} = 3$
Nimkar et al. [166]	FC 72	Aluminum heater	0.5, 0.75, and 1 mm cavity spacing	The active nucleation site density increases with 0.5 mm spacing
C. Hutter et al. [167]	FC-72	Silicon wafer	0.84, 1.2, and 1.5 mm spacing	A slightly increase in the bubble departure diameter is seen for the two widest spacings
Golobič and Gjerkeš [168]	Saturated water	A thin copper or titanium foil	2.6–4.1 mm	The interactions between two nucleation sites reduced the overall activity of both sites

angle of 54° and PF5060 with a contact angle of 10°. They showed that the former's bubble departure diameter and growth period are $D_d \sim g^{-0.5}$ and $t_g \sim g^{-0.93}$ while the latter are $D_d \sim g^{-0.42}$ and $t_g \sim g^{-0.82}$, respectively. Hazi and Markus [52] numerically studied impacts of gravity on the departure frequency and the departure diameter by applying the lattice Boltzmann method. According to their results, the bubble departure frequency and the departure diameter are proportional to $g^{-3/4}$ and $g^{-1/2}$ as depicted in Figs. 21a, b, respectively. Also, Ma et al. [164] numerically investigated microgravity effects on the bubble dynamics parameters from a horizontal hydrophilic surface with constant wall temperature. They found that reducing gravity levels led to an increase in bubble departure diameter and the bubble growth time. It was concluded that the pool boiling curve was significantly influenced by gravity from nucleate boiling to critical heat flux, and from transition boiling to film boiling.

Cavity spacing

Cavity spacing is considered another important factor for controlling the bubble dynamics parameters. Recently, some investigations into the effect of cavity spacing on the bubble dynamics parameters have been carried out. Zhang and Shoji [165] performed experiments pool boiling in distilled water by forming two cylindrical cavities on a heated surface. They found that the bubble departure frequency and diameter increase by increasing a heat flux for the ratio of $\frac{S}{D_d} = 1.5$ which is the ratio of the inter-cavity spacing and the bubble departure diameter. The bubble departure frequency rises by varying this ratio between 1.5 to 2 and decreases while $\frac{S}{D_d} = 3$. Additionally, three surfaces for 64, 100, and 225 cavities with 0.5, 0.75, and 1 mm cavity spacing, respectively, have been prepared by Nimkar et al. [166]. It was concluded that although the bubble departure frequency and diameter are not dependent on cavity spacing, the active nucleation site density increases with 0.5 mm spacing. Hutter et al. [167] investigated the bubble behavior from micro artificial cavities with different spacing (0.84, 1.2, and 1.5 mm spacing between cavities) on a silicon wafer with respect to wall superheat. They found that the bubble departure diameters are lightly larger for the cavities with all spacing by increasing superheat. In another study, Golobič and Gjerkeš [168] considered the spacings between active nucleation sites to be 2.6 to 4.1 mm on a thin copper or titanium foil in saturated water. Based on the results, the interactions between two nucleation sites reduced the overall activity of both sites. A summary of the cavity effects on the bubble behavior in the nucleate boiling is provided in Table 9.

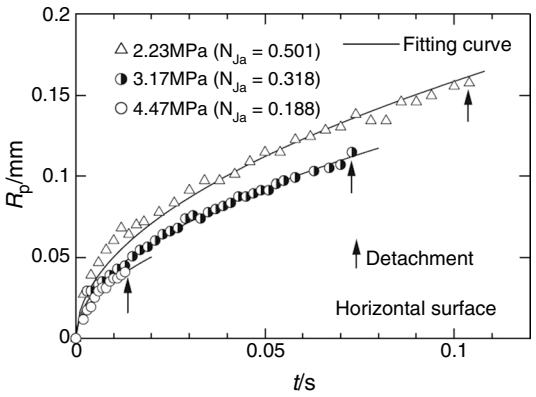

Fig. 22 Comparing the bubble departure radius at different pressures measured by Sakashita [170]

Pressure

The effect of pressure on the bubble dynamics parameters has been studied by some researchers. For example, the bubble growth rate on cylindrical and flat surfaces during water pool boiling at high pressure has been experimentally investigated by Labuntsov et al. [88] and Akiyama et al. [169]. It was concluded that the bubble growth rate decreases by increasing pressure due to the conduction in the vicinity of the bubble base and the evaporation at the triple contact line created at the bubble base. Also, the bubble growth rate for vertical and horizontal surfaces in the period of water pool boiling at pressures from 0.35 to 5 MPa has been studied by Sakashita [170]. Figure 22 shows bubble growth curves at

Table 10 A summary of the pressure effect on the bubble behavior

Reference	Working fluid	Pressure	Bubble behavior
Gong et al. [126]	R170, R600a, and their mixture	0.1, 0.3, and 0.5 MPa	Bubble size reduces with increasing pressure at constant heat flux
Lamas et al. [171]	Water, R134a, ammonia, and R123	0.1–10 bar	The bubble departure diameter slightly decreases with increasing pressure
Hutter et al. [172]	FC-72	1, 1.25, and 1.5 atm	The bubble departure frequency is slightly reduced by increasing pressure, but no effect on the bubble departure diameter
Miglani et al	R-134a	813.6 and 882.5 kPa	The bubble departure diameter reduces and the bubble departure frequency increases with increasing pressure

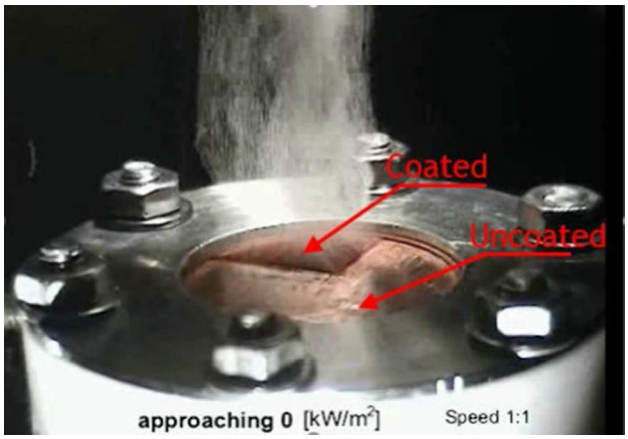

Fig. 23 Difference of bubble generation on coated and bare surfaces [182]

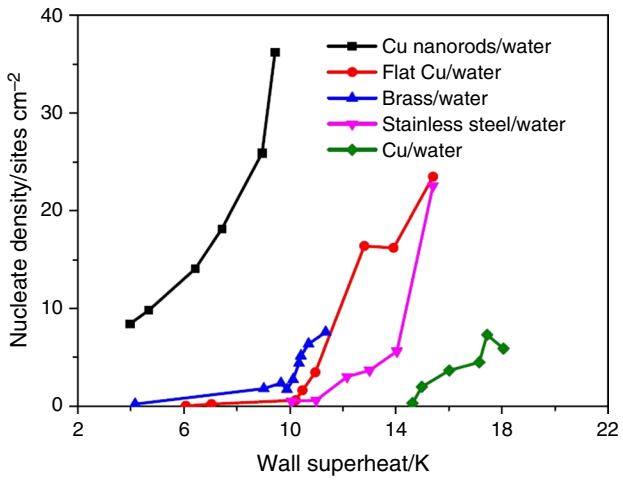

Fig. 24 Variations of nucleation density on different surfaces [180]

three different pressures for the horizontal heating surface. As can be seen, the bubble growth rate becomes slower, and the detachment radius decreases with increasing pressure. Table 10 summarizes some studies focusing on the pressure effects on the bubble behavior.

Surface roughness

The surface roughness is considered to be an important factor in the bubble behavior during boiling as it affects all the parameters such as the bubble departure diameter, frequency, and active nucleation site density [173–177]. McHale and Garimella [152] reported that while a large bubble departure diameter can be achieved on smooth surfaces than that of rough surfaces at a specific heat flux, higher active nucleation site density and departure frequency can be obtained on rough surfaces when compared to smooth surfaces. Additionally, Siedel et al. [156] presented similar results of the bubble departure diameter for rough and polished surfaces. It was also found that the nucleation site density on a heated surface increases by increasing the surface roughness. Also, Suszko and El-Genk [53] performed experiments showing that higher bubble departure frequency and active nucleation site density and smaller departure diameter can be achieved for rough surfaces than smooth surfaces. Nunes et al.[178] investigated the effect of nanocoated surfaces (Al_2O_3 nanoparticles) on the heat transfer coefficient during the pool boiling. Based on the results, the coated surface reduced the heat transfer performance by nearly 29% compared to uncoated surface mostly because of the formation of the fouling resistance on the heated surface. Furthermore, Bovard et al. [72] reported that the bubble departure diameter decreases by increasing the surface roughness for various heated surfaces. Additionally, some experimental investigations [179–181] reported that a higher number of bubbles was observed on nanostructured surfaces than bare surfaces. An illustration of the difference between bubble generation on coated and bare surfaces with the identical heat flux is

Table 11 A summary of bubble departure frequencies and diameters on various surfaces

Author	Surface	Working fluid	Conditions	$D_d/\mu m$	f_d/Hz
Rini el al. [183]	Synthetic diamond plate	FC-72	4–10 W cm^{-2}	400–500	–
Ramaswamy et al. [184]	Micro-channel Si	FC-72	4–12 $K\Delta T_{sat}$	500–700	170–200
El-Genkand Bostanci [185]	Smooth Cu	HFE-7100	0.5 W cm^{-2}	550 ±70	100
Demiray and Kim [186]	Quartz wafer	FC-72	5 K, 16 K subcooling	350–500	–
Nimkar et al. [166, 187]	Smooth Si	FC-72	1–9 W cm^{-2}	260–450	55–68
McHale and Garimella [188, 189]	Rough ITO	FC-72	Surface roughness 0.261–7.51 µm	400–600	100–200
McHale and Garimella [152]	Smooth Al	FC-77	2–11 W cm^{-2}	600–2000	40–150
McHale and Garimella [152]	Rough Al	FC-77	2–11 W cm^{-2}	400–500	80–200
Hutter et al. [172]	Si w/artificial cavities	FC-72	Cavity size 40–100 µm	200–500	40–80
El-Genk and Ali [160]	Micro-porous Cu	PF-5060	0.5 W cm^{-2}	431 ±7	36 ±2

Medical: X-Ray systems

Computer electronics and data centers

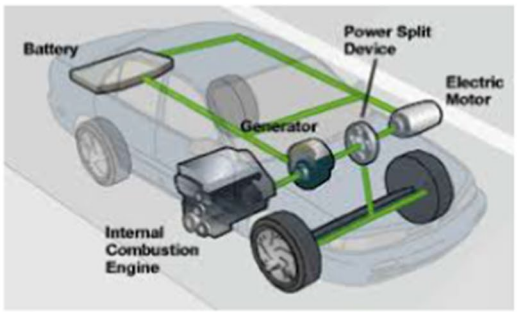

Hybrid vehicles

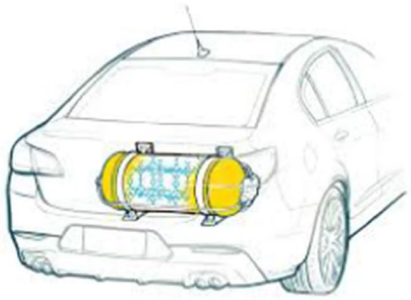

Heat exchangers for Hydrogen storage

Fig. 25 Example applications requiring high heat-flux cooling methods [16]

shown in Fig. 23. Li et al. [180] performed experiments controlling the nucleation site density on the nanostructured surface. As shown in Fig. 24, the nucleation site density on the coated copper surfaces is 30 times higher than bare surfaces. Table 11 shows a summary of bubble departure frequencies and diameters on various surfaces in different studies (Fig. 25).

Application of nucleate boiling

Fundamentals of the bubble growth mechanisms and the bubble dynamics parameters have promoted nucleate boiling heat transfer as an efficient cooling technology for microelectronics, hybrid vehicle power electronics, and heat exchangers for hydrogen storage. This section reviews several applications of nucleate boiling heat transfer that uses various bubble dynamics parameters in the control of the extreme heat flux.

Over recent decades, a critical requirement for novel cooling methods to keep electronic device temperatures securely below specific restrictions associated with each material has been created by intensive miniaturization of electronic components. At the beginning of the 1980s, a transition from the fan-cooled heat sink to various single-phase cooling approaches had taken place. By the mid-1980s, heat dissipation from supercomputers exceeded the capacities of most

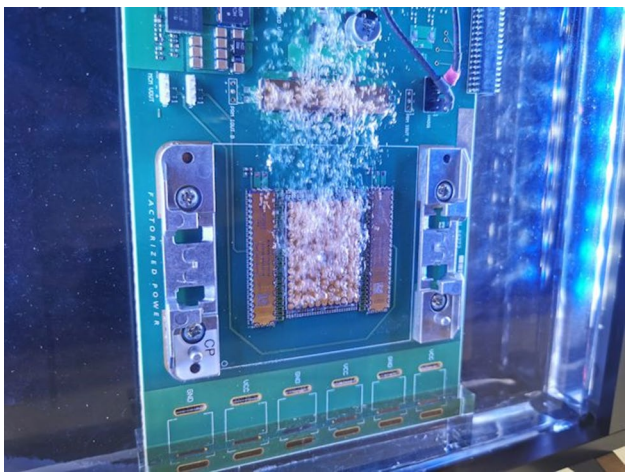

Fig. 26 Two-phase immersion cooling of electronic devices via nucleate boiling

single-phase liquid cooling methods, which approached 100 W cm^{-2} [190]. To obviate this challenge, researchers have started to focus on two-phase cooling systems that take advantage of both sensible and latent heat of the coolant for higher heat removal when compared with single-phase methods. In this cooling strategy, nucleate boiling has been considered the preferred cooling method because a small

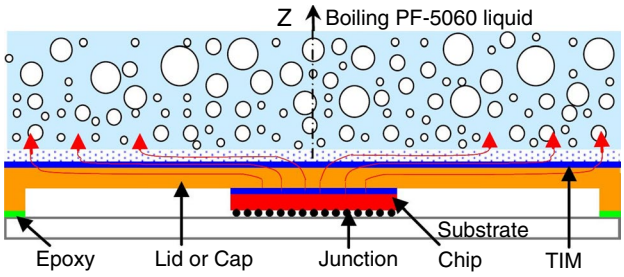

Fig. 27 A schematics of a composite spreader for immersion cooling of high power computer chips by nucleate boiling of dielectric liquids [193]

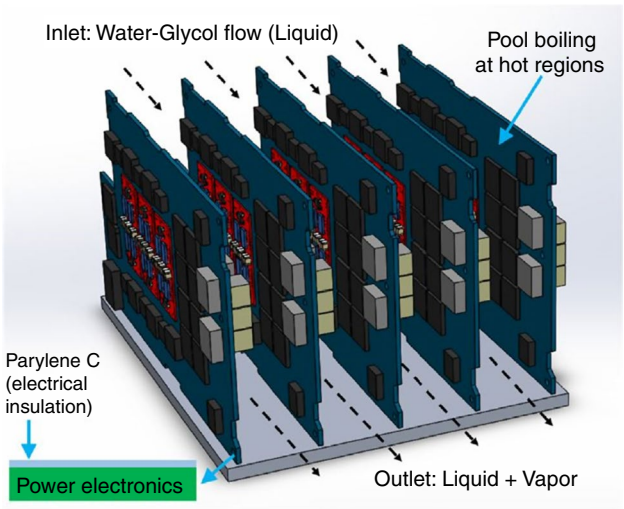

Fig. 28 Schematic of the immersion cooling of electronic device done by Birbarah et al. [194]

increment in wall superheat generally accompanies a significant increase in the wall heat flux [191].

During nucleate boiling, once a bubble is formed, expanded, and detached from a heated surface, it cools down the surface by removing a portion of hot liquid from the surface and replacing it with cold liquid from the bulk as assumed by Forster and Greif [192] or a thin layer of liquid is trapped by the growing bubbles near the surface which then evaporates and transfers considerable energy (proposed by Snyder and Edwards [15]). Regardless of the mechanisms of the bubble growth, the nucleate boiling heat transfer and the bubble growth can remove a great amount of heat from a heated surface. As a result, nucleate boiling heat transfer has been used in some specific cooling systems such as two-phase immersion cooling systems, heat pipes, and spray cooling systems.

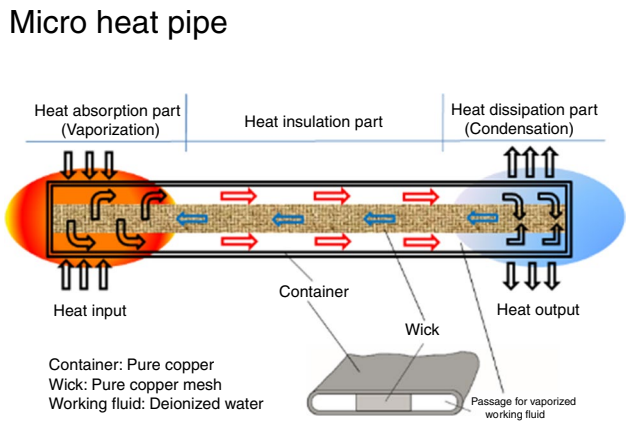

Fig. 29 Working cycle of a micro heat pipe

Two-phase immersion cooling

Two-phase immersion cooling is a new type of cooling technology for data centers. In this method, electronic components are submerged into a bath of water or dielectric heat-transfer liquid, a much better heat conductor than air or oil. With a low boiling point (56 °C vs. 100 °C in water), the fluid boils on the surface of the heat generating components, and rising vapor passively takes care of heat transfer [5]. Two-phase immersion cooling liquids are clean, environmentally friendly, and non-flammable. No pumps and jets are required to keep the hardware at desired operating temperature. Circulation happens passively by the natural process of evaporation and without spending any extra energy. This simplicity eliminates conventional cooling hardware and results in better cooling efficiency. Compared to traditional air, water or oil cooling, this passive process results in the use of much less energy. Figure 26 shows the nucleate boiling in the two-phase immersion cooling.

In two-phase immersion cooling, dielectric liquid has been generally utilized. Cooling CPUs and high-power computer chips using nucleate boiling of dielectric liquids like PF-5060, HFE-7100, and FC-72 benefits not only efficient mitigation of the impact of hot spots but also leads to low and uniform surface temperature. To increase the total heat flux removed via rising the active nucleation site density with two-phase immersion cooling, considerable research has been conducted in aiming to enhance nucleate boiling of dielectric liquids. Ali and El-Genk [193] used a copper spreader with a surface to remove the heat flux from a chip, as shown in Fig. 27. They numerically studied the role of composite spreaders contained Cu micro-porous surfaces and Cu substrates for immersion cooling. Saturation nucleate boiling of PF-5060 dielectric liquid was used to cool down the spreaders. In their results, the total thermal power removed from the surface increases by reducing the

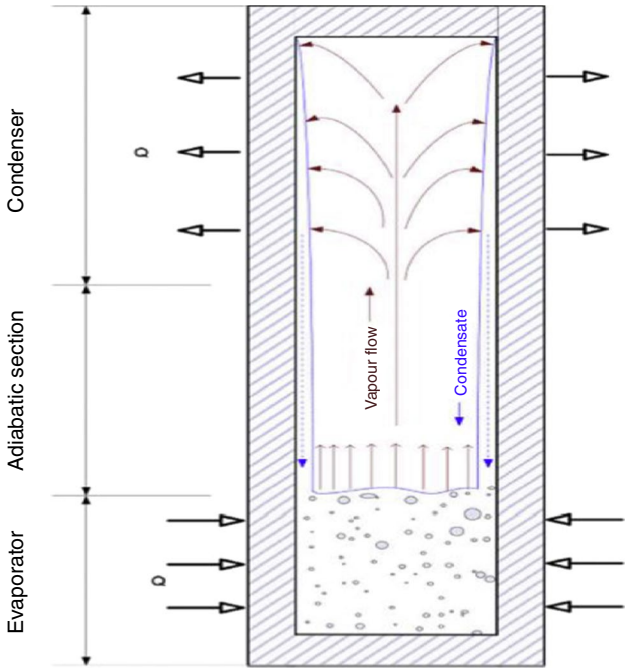

Fig. 30 Working cycle of thermosiphon [196]

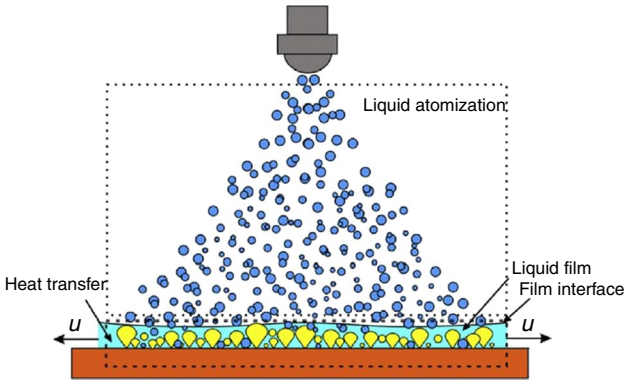

Fig. 31 Schematic of the spray cooling process [218]

thickness of the Cu micro-porous and augmenting Cu substrate's thickness.

Birbarah et al. [194] estimated the convection heat transfer coefficient and heat flux achieved in different dielectric fluids, water, and a 50/50 in volume mixture of water and ethylene glycol (WEG) during both nucleate boiling and natural convection regimes, as shown in Fig. 28. It was reported that water immersion cooling was successful so that a 2-kW power converter works at 97.2% efficiency in deionized water.

Heat pipes

Another application of nucleate boiling in cooling systems is to utilize heat pipes. The working principle of a heat pipe is depicted in Fig. 29. They have been initially used for cooling CPUs and computer devices. Presently, heat pipes are applied in numerous sectors, including heat exchangers, heating, ventilation and air conditioning (HVAC), solar thermal and photovoltaic devices, cryogenic systems, geothermal energy, data-center cooling, residential and commercial refrigeration systems, and waste-heat recovery [195–197]. For instance, Cui et al.[198] numerically modeled vapor bubble growth in a flat-plate heat pipe for microelectronic cooling. They found that the observed bubble (bubble diameter between 10 μm and 0.3 mm) had a growth rate of 0.71 ± 0.19 mm/s. In addition to regular heat pipes, a gravity-assisted heat pipe named thermosyphons has been used for cooling purposes. In thermosyphons, the condensate returns to the evaporator by gravitational forces (Fig. 30). Many investigations have been performed to identify thermal characteristics of thermosyphons, and the most accepted materials in thermosyphons are copper for casing and helium, nitrogen, and argon [199–201]. Additionally, various studies have concentrated on increasing the operating temperature of thermosyphons to accelerate the cooling process from room temperature to extremely low temperatures [202–204].

Spray cooling

Another application of nucleate boiling is in spray cooling systems. A spray cooling system contains liquid droplets generated by pressure or air-assisted atomizers that impinge on a heated surface. Conventionally, sprays were applied to cool extremely heated surfaces like those in steel mills in which film cooling dominates the nucleate boiling. However, modern applications of spray cooling contain high heat flux removal from surfaces while keeping low surface superheats like electronic devices. In this application, nucleate boiling heat transfer is considered a substantial proportion of heat transfer. To determine different aspects of this cooling system, broad studies have been carried out with respect to boiling liquid jets [205–208]. Some investigations have been performed with circular [209–213] as well as planar [214–217] jets in both free-surface and submerged configurations. The schematic of the spray cooling system is shown in Fig. 31.

In addition to jet types, some researchers studied spray cooling systems with different volumetric fluxes (volumetric flow rate per unit area). Depending on the volumetric flux, sprays are categorized as dilute, intermediate, or dense (Fig. 32). A dilute spray has a low volumetric flux with no interaction among bubbles, while dense spray has a high

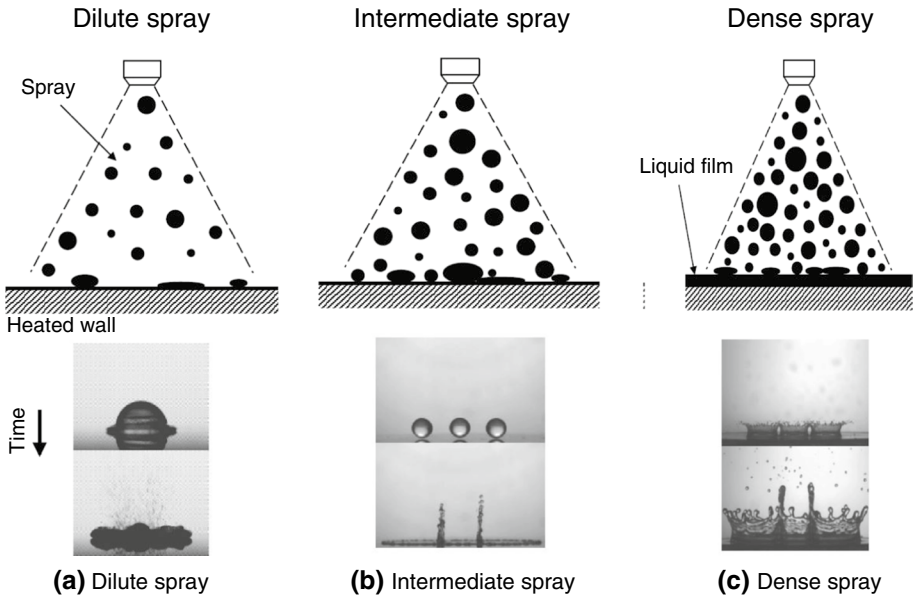

Fig. 32 Schematic of sprays based on different volumetric fluxes [16]

Table 12 Summarizes spray cooling studies with different liquids

Reference	Test fluid	Surface material	Surface size	Nozzle array
Wang et al. [220]	Water	Copper	1×2 cm^2	1×2
Silk et al. [221]	PF-5060	Copper	2 cm^2	2×2
Elston et al. [222]	FC-72	Glass	2.54×2.54 cm^2	4×4
Xie et al. [223]	R-134a	Copper	23.3×16 cm^2	9×6
Yan et al. [224]	R-134a	Copper	15.1×13.5 cm^2	2×2
Lin et al. [225]	FC-72	Copper	2.54×7.6 cm^2	4×12

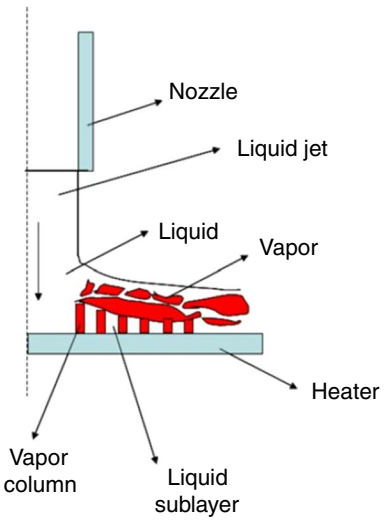

Fig. 33 Mechanism of the spray cooling system used by Narumanchi et al. [191]

volumetric flux in which a thin film is created by accumulating continuous droplets [198]. Rini et al. [219] carried out experiments to understand bubble behavior and nucleate boiling in saturated FC-72 spray cooling while studying the interactions between impinging droplets and bubbles. The results show that the number of secondary nuclei as well as the overall heat transfer coefficient increase as the droplet flux increases, which leads to lower surface temperature for a specific heat flux. Also, S. Narumanchi et al. [191] numerically investigated the turbulent jet impingement in nucleate boiling for power electronics cooling. Besides the interaction between bubbles, the performance of spray cooling systems greatly depends on the used liquid type. To understand its effect, different liquids have been used in spray cooling systems such as water, dielectric fluids (FC-87, FC-77, FC-72, HFE-7100, PF-5020, and PF-5060), refrigerants (R-22, R-113, R-600a, and R-134a), and saline water [16]. Table 12 summarizes spray cooling studies with different liquids (Fig. 33).

Conclusions

The primary goal of this paper is to provide a detailed review on bubble growth characteristics in the nucleate boiling to assist researchers in developing comprehensive boiling heat transfer correlations. We first review two types of bubble growth mechanisms known as homogenous and heterogeneous bubble growth. Next, the bubble dynamics parameters used in different correlations for determining boiling heat transfer coefficient are described and reviewed. Semi-empirical and empirical correlations proposed by various researchers for determining these parameters are completely provided. Then, a detailed review on factors affecting these parameters is performed, and the most recommended correlations were provided in the tables. Furthermore, different applications of nucleate boiling in cooling systems have been reviewed. Based on the review, the following results can be summarized:

1. Although the proposed correlations are able to estimate their own experimental data in a reasonable accuracy, the accuracy of individual correlation is considerably against other researchers' experimental data under same conditions. It happened because these correlations rely on different affecting parameters including thermophysical properties of fluid, gravity level, contact angle, heat flux, and others. Thus, in order to have an accurate prediction, all these parameters must be determined precisely.
2. Active techniques such as applying external electric, magnetic, and ultrasonic field to a working fluid significantly affect the bubble dynamics parameters, resulting in the boiling heat transfer enhancement. For instance, the bubble departure diameter and the bubble growth rate are increased by applying external electric field in a working fluid.
3. Nanofluids as working fluids result in the enhanced boiling heat transfer up to 222% compared with water.

It can be clearly noticed that an overall agreement cannot be observed on the contribution of heat transfer mechanisms and their influences on the bubble growth during boiling. Many suggestions have been provided without any agreement between different studies. Thus, a recommended future study can aim to find the most crucial heat transfer mechanisms in the process of bubble growth. Also, there is a gap in studies regarding nucleate boiling heat transfer enhancement when using active and passive methods especially external electric field, magnetic field, and ultrasonic waves. Furthermore, for the aim of enhancing boiling heat transfer for surface, according to the review studies, porous nanostructures have shown outstanding possibilities in nucleate boiling heat transfer and can be considered effective for managing heat from high heat flux devices. Thus, for obtaining an efficient design regarding future-generation thermal management, a powerful model with an ability to estimate the microscopic heat transfer on micro-porous and nano-porous surfaces and overall heat transfer performance is required.

Acknowledgements This work has been partially supported by the National Science Foundation (Grant #: 1917272).

References

1. Mosavati B, Mosavati M, Kowsary F. Inverse boundary design solution in a combined radiating-free convecting furnace filled with participating medium containing specularly reflecting walls. Int Commun Heat Mass Transf. 2016;76:69–76. https://doi.org/10.1016/j.icheatmasstransfer.2016.04.029.
2. Mosavati B, Mosavati M, Kowsary F. Solution of radiative inverse boundary design problem in a combined radiating-free convecting furnace. Int Commun Heat Mass Transf. 2013;45:130–6. https://doi.org/10.1016/j.icheatmasstransfer.2013.04.011.
3. Mosavati M, Kowsary F, Mosavati B. A novel, noniterative inverse boundary design regularized solution technique using the backward Monte Carlo Method. J Heat Transfer. 2013. https://doi.org/10.1115/1.4022994.
4. Beigzadeh M, Pourfayaz F, Ghazvini M, Ahmadi MH. Energy and exergy analyses of solid oxide fuel cell-gas turbine hybrid systems fed by different renewable biofuels: A comparative study. J Clean Prod. 2021;280:124383. https://doi.org/10.1016/j.jclepro.2020.124383.
5. Fan S, Duan F. A review of two-phase submerged boiling in thermal management of electronic cooling. Int J Heat Mass Transf. 2020;150:119324. https://doi.org/10.1016/j.ijheatmasstransfer.2020.119324.
6. Hetsroni G, Mosyak A, Segal Z, Ziskind G. A uniform temperature heat sink for cooling of electronic devices. Int J Heat Mass Transf. 2002;45:3275–86. https://doi.org/10.1016/S0017-9310(02)00048-0.
7. Selvam RP, Lin L, Ponnappan R. Direct simulation of spray cooling: Effect of vapor bubble growth and liquid droplet impact on heat transfer. Int J Heat Mass Transf. 2006;49:4265–78. https://doi.org/10.1016/j.ijheatmasstransfer.2006.05.009.
8. Cho HJ, Wang EN. Bubble nucleation, growth, and departure: A new, dynamic understanding. Int J Heat Mass Transf. 2019;145:118803. https://doi.org/10.1016/j.ijheatmasstransfer.2019.118803.
9. Mikic BB, Rohsenow WM, Griffith P. On bubble growth rates. Int J Heat Mass Transf. 1970;13:657–66. https://doi.org/10.1016/0017-9310(70)90040-2.
10. Cole R. Bubble frequencies and departure volumes at subatmospheric pressures. AIChE J. 1967;13:779–83. https://doi.org/10.1002/aic.690130434.
11. van Stralen SJD, Sohal MS, Cole R, Sluyter WM. Bubble growth rates in pure and binary systems: Combined effect of relaxation and evaporation microlayers. Int J Heat Mass Transf. 1975;18:453–67. https://doi.org/10.1016/0017-9310(75)90033-2.
12. Nam Y, Aktinol E, Dhir VK, Ju YS. Single bubble dynamics on a superhydrophilic surface with artificial nucleation sites. Int J Heat Mass Transf. 2011;54:1572–7. https://doi.org/10.1016/j.ijheatmasstransfer.2010.11.031.

13. Son G, Dhir VK, Ramanujapu N. Dynamics and heat transfer associated with a single bubble during nucleate boiling on a horizontal surface. J Heat Transfer. 1999;121:623–31. https://doi.org/10.1115/1.2826025.
14. Mukherjee A, Kandlikar SG. Numerical study of single bubbles with dynamic contact angle during nucleate pool boiling. Int J Heat Mass Transf. 2007;50:127–38. https://doi.org/10.1016/j.ijheatmasstransfer.2006.06.037.
15. Kim J. Review of nucleate pool boiling bubble heat transfer mechanisms. Int J Multiph Flow. 2009;35:1067–76. https://doi.org/10.1016/j.ijmultiphaseflow.2009.07.008.
16. Liang G, Mudawar I. Review of spray cooling – Part 1: Single-phase and nucleate boiling regimes, and critical heat flux. Int J Heat Mass Transf. 2017;115:1174–205. https://doi.org/10.1016/j.ijheatmasstransfer.2017.06.029.
17. Liang G, Mudawar I. Review of spray cooling – part 2: High temperature boiling regimes and quenching applications. Int J Heat Mass Transf. 2017;115:1206–22. https://doi.org/10.1016/j.ijheatmasstransfer.2017.06.022.
18. Sadeghi R, Shadloo MS. Three-dimensional numerical investigation of film boiling by the lattice Boltzmann method. Numer Heat Transf Part A Appl. 2017;71:560–74. https://doi.org/10.1080/10407782.2016.1277936.
19. Goodarzi M, Tlili I, Moria H, Cardoso EM, Alkanhal TA, Anqi AE, et al. Boiling flow of graphene nanoplatelets nano-suspension on a small copper disk. Powder Technol. 2021;377:10–9. https://doi.org/10.1016/j.powtec.2020.08.083.
20. Li Z, Sarafraz MM, Mazinani A, Hayat T, Alsulami H, Goodarzi M. Pool boiling heat transfer to CuO-H2O nanofluid on finned surfaces. Int J Heat Mass Transf. 2020;156:119780. https://doi.org/10.1016/j.ijheatmasstransfer.2020.119780.
21. Sarafraz MM, Tlili I, Tian Z, Khan AR, Safaei MR. Thermal analysis and thermo-hydraulic characteristics of zirconia–water nanofluid under a convective boiling regime. J Therm Anal Calorim. 2020;139:2413–22. https://doi.org/10.1007/s10973-019-08435-x.
22. Rashidi S, Hormozi F, Sarafraz MM. Potentials of boiling heat transfer in advanced thermal energy systems. J Therm Anal Calorim. 2020;143:1833–54. https://doi.org/10.1007/s10973-020-09511-3.
23. Rashidi S, Hormozi F, Sarafraz MM. Fundamental and sub-phenomena of boiling heat transfer. J Therm Anal Calorim. 2020;143:1815–32. https://doi.org/10.1007/s10973-020-09468-3.
24. Kamel MS, Al-agha MS, Lezsovits F, Mahian O. Simulation of pool boiling of nanofluids by using Eulerian multiphase model. J Therm Anal Calorim. 2020;142:493–505. https://doi.org/10.1007/s10973-019-09180-x.
25. Liang G, Mudawar I. Pool boiling critical heat flux (CHF) – Part 1: Review of mechanisms, models, and correlations. Int J Heat Mass Transf. 2018;117:1352–67. https://doi.org/10.1016/j.ijheatmasstransfer.2017.09.134.
26. Bankoff SG. Entrapment of gas in the spreading of a liquid over a rough surface. AIChE J. 1958;4:24–6. https://doi.org/10.1002/aic.690040105.
27. Griffith P, Wallis JD. THE ROLE OF SURFACE CONDITIONS IN NUCLEATE BOILING. Cambridge, Mass.: Massachusetts Institute of Technology, 1958.
28. Lorenz JJ, Mikic BB, Rohsenow Warren M. The effects of surface conditions on boiling characteristics. Cambridge, Mass.: M.I.T. Engineering Projects Laboratory, 1972.
29. Hsu YY. On the size range of active nucleation cavities on a heating surface. J Heat Transfer. 1962;84:207–13. https://doi.org/10.1115/1.3684339.
30. Alavi Fazel SA, Shafaee SB. Bubble dynamics for nucleate pool boiling of electrolyte solutions. J Heat Transfer. 2010;132:1–7. https://doi.org/10.1115/1.4001315.
31. Zeng LZ, Klausner JF, Mei R. A unified model for the prediction of bubble detachment diameters in boiling systems- I. Pool boiling. Int J Heat Mass Transf. 1993;36:2261–70. https://doi.org/10.1016/S0017-9310(05)80111-5.
32. Kocamustafaogullari G. Pressure dependence of bubble departure diameter for water. Int Commun Heat Mass Transf. 1983;10:501–9. https://doi.org/10.1016/0735-1933(83)90057-X.
33. Mohanty RL, Das MK. A critical review on bubble dynamics parameters influencing boiling heat transfer. Renew Sustain Energy Rev. 2017;78:466–94. https://doi.org/10.1016/j.rser.2017.04.092.
34. Faghri A, Zhang Y. Boiling chapter-Transport Phenomenon in Multiphase Systems. Transp Phenom Multiph Syst, Elsevier 2006. pp. 765–852.
35. Plesset MS, Zwick SA. The growth of vapor bubbles in superheated liquids. J Appl Phys. 1954;25:493–500. https://doi.org/10.1063/1.1721668.
36. Miyatake O, Tanaka I, Lior N. A simple universal equation for bubble growth in pure liquids and binary solutions with a non-volatile solute. Int J Heat Mass Transf. 1997;40:1577–84. https://doi.org/10.1016/S0017-9310(96)00224-4.
37. Theofanous TG, Patel PD. Universal relations for bubble growth. Int J Heat Mass Transf. 1976;19:425–9. https://doi.org/10.1016/0017-9310(76)90098-3.
38. Forster HK, Zuber N. Growth of a vapor bubble in a superheated liquid. J Appl Phys. 1954;25:474–8. https://doi.org/10.1063/1.1721664.
39. Zuber N. The dynamics of vapor bubbles in nonuniform temperature fields. Int J Heat Mass Transf. 1961;2:83–98. https://doi.org/10.1016/0017-9310(61)90016-3.
40. Carey VP. Liquid-Vapor Phase-Change Phenomena: An Introduction to the Thermophysics of Vaporization and Condensation Processes in Heat Transfer Equipment, Second Edition. Taylor and Francis; 2008.
41. Guichet V, Almahmoud S, Jouhara H. Nucleate pool boiling heat transfer in wickless heat pipes (two-phase closed thermosyphons): A critical review of correlations. Therm Sci Eng Prog. 2019;13:100384. https://doi.org/10.1016/j.tsep.2019.100384.
42. Cole R, Shulman HL. Bubble growth rates at high Jakob numbers. Int J Heat Mass Transf. 1966;9:1377–90. https://doi.org/10.1016/0017-9310(66)90135-9.
43. Chi-Yeh H, Griffith P. The mechanism of heat transfer in nucleate pool boiling-Part I. Bubble initiaton, growth and departure. Int J Heat Mass Transf. 1965;8:887–904. https://doi.org/10.1016/0017-9310(65)90073-6.
44. Howell JR, Siegel R. Incipience, growth, and detachment of boiling bubbles in saturated water from artificial nucleation sites of known geometry and size. Int Heat Transf Conf. 2019;3:12–23. https://doi.org/10.1615/ihtc3.1120.
45. Eastman RE. Dynamics of bubble departure. AIAA Pap., AIAA19th Thermophysics Conference; 1984. https://doi.org/10.2514/6.1984-1707.
46. W. Fritz, "Maximum volume of vapor bubbles," Physikalische Zeitschrift, vol. 36, pp. 379–384, 1935. - Open Access Library n.d. http://www.oalib.com/references/14278337 (accessed January 9, 2020).
47. Staniszewski B. Nucleate boiling bubble growth and departure, Cambridge, Mass.: Massachusetts Institute of Technology. 1959.
48. Ardron KH, Giustini G, Walker SP. Prediction of dynamic contact angles and bubble departure diameters in pool boiling using equilibrium thermodynamics. Int J Heat Mass Transf. 2017;114:1274–94. https://doi.org/10.1016/j.ijheatmasstransfer.2017.07.013.
49. Cho YJ, Yum SB, Lee JH, Park GC. Development of bubble departure and lift-off diameter models in low heat flux and low flow velocity conditions. Int J Heat Mass Transf.

2011;54:3234–44. https://doi.org/10.1016/j.ijheatmasstransfer.2011.04.007.
50. Basu N, Warrier GR, Dhir VK. Wall heat flux partitioning during subcooled flow boiling: Part 1 - Model development. J Heat Transfer. 2005;127:131–40. https://doi.org/10.1115/1.1842784.
51. Kocamustafaogullari G, Ishii M. Aire interfaciale et densite de sites de nucleation dans les systemes en ebullition. Int J Heat Mass Transf. 1983;26:1377–87. https://doi.org/10.1016/S0017-9310(83)80069-6.
52. Hazi G, Markus A. On the bubble departure diameter and release frequency based on numerical simulation results. Int J Heat Mass Transf. 2009;52:1472–80. https://doi.org/10.1016/j.ijheatmasstransfer.2008.09.003.
53. Suszko A, El-Genk MS. Saturation boiling of PF-5060 on rough Cu surfaces: Bubbles transient growth, departure diameter and detachment frequency. Int J Heat Mass Transf. 2015;91:363–73. https://doi.org/10.1016/j.ijheatmasstransfer.2015.07.083.
54. Borinshansky V, Fokin FS. Heat transfer and hydrodynamics in steam generators, Trudy TsKTI, 1963.
55. Ruckenstein R. Recent trends in boiling heat and mass transfer. Appl Mech Rev 1964;17:663–72.
56. Hatton P, Hall IS. Photographic study of boiling on prepared surfaces. In: Proceedings of the 3rd international heat transfer conference, AIChE, vol. 4, no. 2, 1966, p. 24–37.
57. Cole RRW. Correlation of bubble departure diameters for boiling of saturated liquids. Chem Eng Prog Symp Ser. 1969;65:211–3.
58. Van Stralen SJD, Zijl W. Fundamental developments in bubble dynamics. In: Proceedings of the 6th international heat transfer conference, vol. 6, 1978, p. 429–50.
59. Golorin VS, Kolchugin BA, Zakharova EA. Investigation of the mechanism of nucleate boiling of ethyl alcohol and benzene by means of high speed motionpicture photography. Heat Transf Sov Res 1978;10:79–98.
60. Kutateladze SS, Gogonin II. Growth rate and detachment diameter of a vapor bubble in free convection boiling of a saturated liquids. High Temp 1979;17:667–71.
61. Gorenflo D, Knabe V, Bieling V. Bubble density on surfaces with nucleate boiling-Its influences on heat transfer. In: Proceedings of the 8th international heat transfer conference, vol. 4, 1986, p. 1995–2000.
62. Wenzel U, Ulrich. Saturated pool boiling and subcooled flow boiling of mixtures at atmospheric pressure, Thesis (PhD–Chemical and Materials Engineering)–University of Auckland, 1992.
63. Zeng LZ, Klausner JF, Bernhard DM, Mei R. A unified model for the prediction of bubble detachment diameters in boiling systems-II. Flow boiling. Int J Heat Mass Transf. 1993;36:2271–9. https://doi.org/10.1016/S0017-9310(05)80112-7.
64. Yang C, Wu Y, Yuan X, Ma C. Study on bubble dynamics for pool nucleate boiling. Int J Heat Mass Transf. 2000;43:203–8. https://doi.org/10.1016/s0017-9310(99)00132-5.
65. Lee HC, Do OB, Bae SW, Kim MH. Single bubble growth in saturated pool boiling on a constant wall temperature surface. Int J Multiph Flow. 2003;29:1857–74. https://doi.org/10.1016/j.ijmultiphaseflow.2003.09.003.
66. Jamialahmadi M, Helalizadeh A, Müller-Steinhagen H. Pool boiling heat transfer to electrolyte solutions. Int J Heat Mass Transf. 2004;47:729–42. https://doi.org/10.1016/j.ijheatmasstransfer.2003.07.025.
67. Kim J, Kim MH. On the departure behaviors of bubble at nucleate pool boiling. Int J Multiph Flow. 2006;32:1269–86. https://doi.org/10.1016/j.ijmultiphaseflow.2006.06.010.
68. Fazel SAA, Shafaee SB. Bubble dynamics for nucleate poll boiling of electrolyte solutions. ASME J Heat Transf. 2010;132(2):815021–7.
69. Phan HT, Caney N, Marty P, Colasson S, Gavillet J. A model to predict the effect of contact angle on the bubble departure diameter during heterogeneous boiling. Int Commun Heat Mass Transf. 2010;37:964–9. https://doi.org/10.1016/j.icheatmasstransfer.2010.06.024.
70. Lamas MI, Jabardo JMS, Arce A, Farinas P. Numerical analysis of the bubble detachment diameter in nucleate boiling. In: Proceedings of the 6th European Therm Sci Conf, J Phy: Conf Series 395, 2012.
71. Hamzekhani S, Maniavi Falahieh M, Akbari A. Bubble departure diameter in nucleate pool boiling at saturation: Pure liquids and binary mixtures. Int J Refrig. 2014;46:50–8. https://doi.org/10.1016/j.ijrefrig.2014.07.003.
72. Bovard S, Asadinia H, Hosseini G, Alavi Fazel SA. Investigation and experimental analysis of the bubble departure diameter in pure liquids on horizontal cylindrical heater. Heat Mass Transf Und Stoffuebertragung. 2017;53:1199–210. https://doi.org/10.1007/s00231-016-1885-3.
73. Ünal HC. Maximum bubble diameter, maximum bubble-growth time and bubble-growth rate during the subcooled nucleate flow boiling of water up to 17.7 MN/m2. Int J Heat Mass Transf. 1976;19:643–9. https://doi.org/10.1016/0017-9310(76)90047-8.
74. Bae BU, Yun BJ, Euh DJ, Song CH, Yoon HY. Development of CFD Code for Subcooled Boiling Two-Phase Flow with Modeling of the Interfacial Area Transport Equation (KAERI/TR–3679/2008). Republic of Korea. 2008.
75. Gupta MK, Sharma DS, Lakhera VJ. Vapor bubble formation, forces, and induced vibration: A review. Appl Mech Rev. 2016. https://doi.org/10.1115/1.4033622.
76. Gaertner RF, Westwater JW. Population of active sites in nucleate boiling heat transfer.Chem Eng Prog Symp Ser 1960;56:39–48.
77. Mikic BB, Rohsenow WM. A new correlation of pool-boiling data including the effect of heating surface characteristics. J Heat Transfer. 1969;91:245–50. https://doi.org/10.1115/1.3580136.
78. Zou L, Jones BG. Thermal interaction effect on nucleation site distribution in subcooled boiling. Int J Heat Mass Transf. 2012;55:2822–8. https://doi.org/10.1016/j.ijheatmasstransfer.2012.02.044.
79. Hibiki T, Ishii M. Active nucleation site density in boiling systems. Int J Heat Mass Transf. 2003;46:2587–601. https://doi.org/10.1016/S0017-9310(03)00031-0.
80. Bier K, Gorenflo D, Salem M, Tanes Y. Pool boiling heat transfer and size of active nucleation centers for horizontal plates with different surface roughness. In: Proceedings of the 6th heat transfer conference. Toronto, vol. 1, 1978, p. 151–56.
81. Cornwell K, Brown RD. Boiling surface topography. In: Proceedings of the 6th international heat transfer conference. Toronto, vol. 1, 1978, p. 157–61.
82. Paul DD, Abdel-Khalik SI. A statistical analysis of saturated nucleate boiling along a heated wire. Int J Heat Mass Transf. 1983;26:509–19. https://doi.org/10.1016/0017-9310(83)90002-9.
83. Yang SR, Kim RH. A mathematical model of the pool boiling nucleation site density in terms of the surface characteristics. Int J Heat Mass Transf. 1988;31:1127–35. https://doi.org/10.1016/0017-9310(88)90055-5.
84. Wang CH, Dhir VK. Effect of surface wettability on active nucleation site density during pool boiling of water on a vertical surface. J Heat Transfer. 1993;115:659–69. https://doi.org/10.1115/1.2910737.
85. Benjamin RJ, Balakrishnan AR. Nucleation site density in pool boiling of saturated pure liquids: effect of surface microroughness and surface and liquid physical properties. Exp Therm Fluid Sci. 1997;15:32–42. https://doi.org/10.1016/S0894-1777(96)00168-9.
86. Sakashita H, Kumada T. Method for predicting boiling curves of saturated nucleate boiling. Int J Heat Mass Transf. 2001;44:673–82. https://doi.org/10.1016/S0017-9310(00)00104-6.

87. Hsu YY, Graham RW. Transport processes in boiling and two-phase systems. Chaps 5 and 6, 2. New York: Hemisphere; 1976.
88. Labuntsov DA, Kolchugin BA, Golovin VS, Zakharova EA, Vladimirova LN. Study of the growth of bubbles during boiling of saturated water within a wide range of pressures by means of high-speed moving pictures. UCS 1964;536.423(1):404–9.
89. Van Stralen SJD, Sluyter WM. Local temperature fluctuations in saturated pool boiling of pure liquids and binary mixtures. Int J Heat Mass Transf. 1969. https://doi.org/10.1016/0017-9310(69)90061-1.
90. Hamzekhani S, Falahieh MM, Kamalizadeh MR, Nazari Z. Experimental study on bubble departure frequency for pool boiling of water/NaCl solutions. Heat Mass Transf Und Stoffuebertragung. 2015;51:1313–20. https://doi.org/10.1007/s00231-015-1502-x.
91. Akiyama M, Tachibana F, Ogawa N. Effect of pressure on bubble growth in pool boiling. Bull JSME. 1969;12:1121–8. https://doi.org/10.1299/jsme1958.12.1121.
92. Chen DQ, Pan LM, Yuan DW, Zhang H, Xu JH, Huang YP. The nature of bubble growth under different system pressures in a narrow channel. Nucl Eng Des. 2011;241:785–91. https://doi.org/10.1016/j.nucengdes.2010.12.013.
93. Cooper MG. The microlayer and bubble growth in nucleate pool boiling. Int J Heat Mass Transf. 1969;12:915–33. https://doi.org/10.1016/0017-9310(69)90155-0.
94. Zhao YH, Masuoka T, Tsuruta T. Unified theoretical prediction of fully developed nucleate boiling and critical heat flux based on a dynamic microlayer model. Int J Heat Mass Transf. 2002;45:3189–97. https://doi.org/10.1016/S0017-9310(02)00022-4.
95. Yun BJ, Splawski A, Lo S, Song CH. Prediction of a subcooled boiling flow with advanced two-phase flow models. Nucl Eng Des. 2012;253:351–9. https://doi.org/10.1016/j.nucengdes.2011.08.067.
96. Jakob and Linke. Heat transfer from a horizontal plate. Forsch Geb Ing. 1933;4:75–81. https://doi.org/10.1002/cjce.5450670324.
97. Jakob MFW. Versuche uber den verdampfungsvorgang. Forsch Auf Dem Geb Des Ing. 1935;2:435–47. https://doi.org/10.1007/3-540-69835-3_16.
98. Peebles FN, Garber HJ. Study on motion of gas bubbles in liquids. Chem Eng Prog 1953;49:88–97.
99. McFadden PW, Grassmann P. The relation between bubble frequency and diameter during nucleate pool boiling. Int J Heat Mass Transf. 1962;5:169–73. https://doi.org/10.1016/0017-9310(62)90009-1.
100. Zuber N. Nucleate boiling. The region of isolated bubbles and the similarity with natural convection. Int J Heat Mass Transf. 1963. https://doi.org/10.1016/0017-9310(63)90029-2.
101. Jakob M. Heat Transfer, Chapter 29, 1. New York: Wiley and Sons; 1949.
102. Jakob L. Heat transfer from a horizontal plate. Forsch Geb Ing. 1933;4:75–81.
103. Ivey HJ. Relationships between bubble frequency, departure diameter and rise velocity in nucleate boiling. Int J Heat Mass Transf. 1967;10:1023–40. https://doi.org/10.1016/0017-9310(67)90118-4.
104. Malenkov IG. Detachment frequency as a function of size for vapor bubbles. J Eng Phys. 1971;20:704–8. https://doi.org/10.1007/BF01122590.
105. Katto Y, Yokoya S. Behavior of a Vapor Mass in Saturated Nucleate and Transitional Pool Boiling. Trans Japan Soc Mech Eng. 1975;41:294–305. https://doi.org/10.1299/kikai1938.41.294.
106. Stephan K. Heat transfer in condensation and boiling. New York: Springer; 1992.
107. Kumada T, Sakashita H, Yamagishi H. Pool boiling heat transfer-I. Measurement and semi-empirical relations of detachment frequencies of coalesced bubbles. Int J Heat Mass Transf. 1995;38:969–77. https://doi.org/10.1016/0017-9310(94)00224-J.
108. Sakashita H, Ono A. Boiling behaviors and critical heat flux on a horizontal plate in saturated pool boiling of water at high pressures. Int J Heat Mass Transf. 2009;52:744–50. https://doi.org/10.1016/j.ijheatmasstransfer.2008.06.040.
109. Miglani A, Joo D, Basu S, Kumar R. Nucleation dynamics and pool boiling characteristics of high pressure refrigerant using thermochromic liquid crystals. Int J Heat Mass Transf. 2013;60:188–200. https://doi.org/10.1016/j.ijheatmasstransfer.2012.12.054.
110. Cheng L, Mewes D, Luke A. Boiling phenomena with surfactants and polymeric additives: A state-of-the-art review. Int J Heat Mass Transf. 2007;50:2744–71. https://doi.org/10.1016/j.ijheatmasstransfer.2006.11.016.
111. Saha SK, Ranjan H, Emani MS, Bharti AK. Two-phase heat transfer enhancement. Springer, 2020.
112. Gao M, Cheng P, Quan X. An experimental investigation on effects of an electric field on bubble growth on a small heater in pool boiling. Int J Heat Mass Transf. 2013;67:984–91. https://doi.org/10.1016/j.ijheatmasstransfer.2013.08.098.
113. Chen F, Peng Y, Song YZ, Chen M. EHD behavior of nitrogen bubbles in DC electric fields. Exp Therm Fluid Sci. 2007;32:174–81. https://doi.org/10.1016/j.expthermflusci.2007.03.006.
114. Dong W, Li RY, Yu HL, Yan YY. An investigation of behaviours of a single bubble in a uniform electric field. Exp Therm Fluid Sci. 2006;30:579–86. https://doi.org/10.1016/j.expthermflusci.2005.12.003.
115. Ogata J, Yabe A. Augmentation of boiling heat transfer by utilizing the EHD effect-EHD behaviour of boiling bubbles and heat transfer characteristics. Int J Heat Mass Transf. 1993;36:783–91. https://doi.org/10.1016/0017-9310(93)80054-X.
116. Xu Y, Karayiannis TG. Electric field effect in boiling heat transfer. part B: electrode geometry. J Enhanc Heat Transf. 1998;5:231–47. https://doi.org/10.1615/jenhheattransf.v5.i4.20.
117. Madadnia J, Koosha H. Electrohydrodynamic effects on characteristic of isolated bubbles in the nucleate pool boiling regime. Exp Therm Fluid Sci. 2003;27:145–50. https://doi.org/10.1016/S0894-1777(02)00258-3.
118. Kweon YC, Kim MH. Experimental study on nucleate boiling enhancement and bubble dynamic behavior in saturated pool boiling using a nonuniform de electric field. Int J Multiph Flow. 2000;26:1351–68. https://doi.org/10.1016/S0301-9322(99)00090-7.
119. Pascual CC, Jeter SM, Abdel-Khalik SI. A statistical analysis of EHD-enhanced nucleate boiling along a heated wire. Int J Heat Mass Transf. 2001;44:1201–12. https://doi.org/10.1016/S0017-9310(00)00149-6.
120. Siedel S, Cioulachtjian S, Robinson AJ, Bonjour J. Electric field effects during nucleate boiling from an artificial nucleation site. Exp Therm Fluid Sci. 2011;35:762–71. https://doi.org/10.1016/j.expthermflusci.2010.06.006.
121. Chen F, Liu D, Song Y. Visualization of a single boiling bubble in a DC electric field. vol. 2, American Society of Mechanical Engineers Digital Collection; 2012, p. 245–52. https://doi.org/10.1115/FEDSM2012-72493.
122. Rahmati P, Ebrahimi-Dehshali M, Hakkaki-Fard A. Enhancement of pool boiling heat transfer using ferromagnetic beads in a variable magnetic field. Appl Therm Eng. 2020;164:114439. https://doi.org/10.1016/j.applthermaleng.2019.114439.
123. Junhong L, Jianming G, Zhiwei L, Hui L. Experiments and mechanism analysis of pool boiling heat transfer enhancement with water-based magnetic fluid. Heat Mass Transf Und

Stoffuebertragung. 2004;41:170–5. https://doi.org/10.1007/s00231-004-0529-1.
124. Abdollahi A, Salimpour MR, Etesami N. Experimental analysis of magnetic field effect on the pool boiling heat transfer of a ferrofluid. Appl Therm Eng. 2017;111:1101–10. https://doi.org/10.1016/j.applthermaleng.2016.10.019.
125. Khooshechin M, Fathi S, Salimi F, Ovaysi S. The influence of surfactant and ultrasonic processing on improvement of stability and heat transfer coefficient of CuO nanoparticles in the pool boiling. Int J Heat Mass Transf. 2020;154:119783. https://doi.org/10.1016/j.ijheatmasstransfer.2020.119783.
126. Gong M, Wu Y, Ding L, Cheng K, Wu J. Visualization study on nucleate pool boiling of ethane, isobutane and their binary mixtures. Exp Therm Fluid Sci. 2013;51:164–73. https://doi.org/10.1016/j.expthermflusci.2013.07.011.
127. Gao W, Qi J, Yang X, Zhang J, Wu D. Experimental investigation on bubble departure diameter in pool boiling under subatmospheric pressure. Int J Heat Mass Transf. 2019;134:933–47. https://doi.org/10.1016/j.ijheatmasstransfer.2019.01.024.
128. Goodarzi M, Tlili I, Moria H, Abdullah Alkanhal T, Ellahi R, Anqi AE, et al. Boiling heat transfer characteristics of graphene oxide nanoplatelets nano-suspensions of water-perfluorohexane (C6F14) and water-n-pentane. Alexandria Eng J. 2020;59:4511–21. https://doi.org/10.1016/j.aej.2020.08.003.
129. Li Z, Mazinani A, Hayat T, Al-Rashed AAAA, Alsulami H, Goodarzi M, et al. Transient pool boiling and particulate deposition of copper oxide nano-suspensions. Int J Heat Mass Transf. 2020;155:119743. https://doi.org/10.1016/j.ijheatmasstransfer.2020.119743.
130. Safaei MR, Tlili I, Gholamalizadeh E, Abbas T, Alkanhal TA, Goodarzi M, et al. Thermal analysis of a binary base fluid in pool boiling system of glycol–water alumina nano-suspension. J Therm Anal Calorim. 2020. https://doi.org/10.1007/s10973-020-09911-5.
131. Salehi H, Hormozi F. Prediction of Al2O3–water nanofluids pool boiling heat transfer coefficient at low heat fluxes by using response surface methodology. J Therm Anal Calorim. 2019;137:1069–82. https://doi.org/10.1007/s10973-018-07993-w.
132. Mukherjee S, Mishra PC, Chaudhuri P. Pool boiling performance of aqueous Al_2O_3 and TiO_2 nanofluids on a horizontally placed flat polished surface: an experimental investigation. J Therm Anal Calorim. 2020. https://doi.org/10.1007/s10973-020-09995-z.
133. Wang D, Quan X, Liu C, Cheng P. An experimental investigation on periodic single bubble growth and departure from a small heater submerged in a nanofluid containing moderately hydrophilic nanoparticles. Int Commun Heat Mass Transf. 2018;95:1–8. https://doi.org/10.1016/j.icheatmasstransfer.2018.03.016.
134. Cieliski JT, Krygier K. Augmentation of the critical heat flux in water-Al_2O_3, water-TiO_2 and water-Cu nanofluids MATEC Web of Conferences Volume 18, 101 EUROTHERM Seminar – Transport Phenomena in Multiphase Systems, 2014.
135. Truong BH. Determination of pool boiling Critical Heat Flux enhancement in nanofluids. ASME Int. Mech. Eng. Congr. Expo. Proc., vol. 8 PART A, American Society of Mechanical Engineers Digital Collection; 2008, p. 289–99. https://doi.org/10.1115/IMECE2007-41697.
136. Ali HM, Generous MM, Ahmad F, Irfan M. Experimental investigation of nucleate pool boiling heat transfer enhancement of TiO_2-water based nanofluids. Appl Therm Eng. 2017;113:1146–51. https://doi.org/10.1016/j.applthermaleng.2016.11.127.
137. Milanova D, Kumar R. Heat transfer behavior of silica nanoparticles in pool boiling experiment. Journal of Heat Transfer, vol. 130, American Society of Mechanical Engineers Digital Collection; 2008. https://doi.org/10.1115/1.2787020.
138. Rainho Neto A, Oliveira JLG, Passos JC. Heat transfer coefficient and critical heat flux during nucleate pool boiling of water in the presence of nanoparticles of alumina, maghemite and CNTs. Appl Therm Eng. 2017;111:1493–506. https://doi.org/10.1016/j.applthermaleng.2016.06.130.
139. Bang IC, Heung CS. Boiling heat transfer performance and phenomena of Al2O 3-water nano-fluids from a plain surface in a pool. Int J Heat Mass Transf. 2005;48:2407–19. https://doi.org/10.1016/j.ijheatmasstransfer.2004.12.047.
140. You SM, Kim JH, Kim KH. Effect of nanoparticles on critical heat flux of water in pool boiling heat transfer. Appl Phys Lett. 2003;83:3374–6. https://doi.org/10.1063/1.1619206.
141. Kim HD, Kim J, Kim MH. Experimental studies on CHF characteristics of nano-fluids at pool boiling. Int J Multiph Flow. 2007;33:691–706. https://doi.org/10.1016/j.ijmultiphaseflow.2007.02.007.
142. Kim SJ, Bang IC, Buongiorno J, Hu LW. Study of pool boiling and critical heat flux enhancement in nanofluids. vol. 55, no. 2, 2007.
143. Padhye R, McCollum J, Korzeniewski C, Pantoya ML. Examining Hydroxyl-Alumina Bonding toward Aluminum Nanoparticle Reactivity. J Phys Chem C. 2015;119:26547–53. https://doi.org/10.1021/acs.jpcc.5b08408.
144. Hiswankar SC, Kshirsagar JM. Determination Of Critical Heat Flux In Pool Boiling Using ZnO Nanofluids. Int J Eng Res Tech (IJERT) 2013;2(7).
145. Kathiravan R, Kumar R, Gupta A, Chandra R. Preparation and pool boiling characteristics of copper nanofluids over a flat plate heater. Int J Heat Mass Transf. 2010;53:1673–81. https://doi.org/10.1016/j.ijheatmasstransfer.2010.01.022.
146. Alavi Fazel SA, Mahboobpour M. Pool boiling heat transfer in monoethyleneglycol aqueous solutions. Exp Therm Fluid Sci. 2013;48:177–83. https://doi.org/10.1016/j.expthermflusci.2013.02.021.
147. Tong W, Wu C, Toh KC, Duan F. Experimental study of bubble dynamics in highly wetting dielectric liquid pool boiling through high-speed video. 2016 15th IEEE Intersociety Conference on Thermal and Thermomechanical Phenomena in Electronic Systems (ITherm), 2016,p. 359–63. https://doi.org/10.1109/ITHERM.2016.7517571.
148. Gong S, Cheng P. Lattice Boltzmann simulation of periodic bubble nucleation, growth and departure from a heated surface in pool boiling. Int J Heat Mass Transf. 2013;64:122–32. https://doi.org/10.1016/j.ijheatmasstransfer.2013.03.058.
149. Judd RL, Hwang KS. A comprehensive model for nucleate pool boiling heat transfer including microlayer evaporation. J Heat Transfer. 1976;98:623–9. https://doi.org/10.1115/1.3450610.
150. Nakayama W, Daikoku T, Kuwahara H, Nakajima T. Dynamic model of enhanced boiling heat transfer on porous surfaces: Part I: Experimental investigation. J Heat Transfer. 1980;102:445–50. https://doi.org/10.1115/1.3244320.
151. Chien LH, Webb RL. Measurement of bubble dynamics on an enhanced boiling surface. Exp Therm Fluid Sci. 1998;16:177–86. https://doi.org/10.1016/S0894-1777(97)10017-6.
152. McHale JP, Garimella SV. Bubble nucleation characteristics in pool boiling of a wetting liquid on smooth and rough surfaces. Int J Multiph Flow. 2010;36:249–60. https://doi.org/10.1016/j.ijmultiphaseflow.2009.12.004.
153. Zuber N, Hydrodynamics aspects of boiling heat transfer, US AEC Report AECU 4439, 1959.
154. Dhir VK, Abarajith HS, Li D. Bubble dynamics and heat transfer during pool and flow boiling. Heat Transf Eng. 2007;28:608–24. https://doi.org/10.1080/01457630701266421.
155. Qiu DM, Dhir VK, Chao D, Hasan MM, Neumann E, Yee G, et al. Single-bubble dynamics during pool boiling under low

gravity conditions. J Thermophys Heat Transf. 2002;16:336–45. https://doi.org/10.2514/2.6710.
156. Siedel S, Cioulachtjian S, Bonjour J. Experimental analysis of bubble growth, departure and interactions during pool boiling on artificial nucleation sites. Exp Therm Fluid Sci. 2008;32:1504–11. https://doi.org/10.1016/j.expthermflusci.2008.04.004.
157. Mukherjee A, Kandlikar SG. Effect of dynamic contact angle on single bubbles during nucleate pool boiling. American Society of Mechanical Engineers, Heat Transfer Division. HTD, vol. 375, American Society of Mechanical Engineers (ASME); 2004, p. 555–62. https://doi.org/10.1115/IMECE2004-59976.
158. Mukherjee A, Dhir VK. Study of lateral merger of vapor bubbles during nucleate pool boiling. J Heat Transfer. 2004;126:1023–39. https://doi.org/10.1115/1.1834614.
159. Mukherjee A, Mass SK-IJ of H and, 2007 undefined. Numerical study of single bubbles with dynamic contact angle during nucleate pool boiling. Int J Heat Mass Tran. 2007;50(1–2):127–38.
160. El-Genk MS, Ali AF. Saturation boiling on MPC: Effects of thickness, inclination angle, transient bubble growth, and nucleation site density. Multiph Sci Technol. 2013;25:201–36. https://doi.org/10.1615/MultScienTechn.v25.i2-4.80.
161. Phan HT, Caney N, Marty P, Colasson S, Gavillet J. Surface wettability control by nanocoating: The effects on pool boiling heat transfer and nucleation mechanism. Int J Heat Mass Transf. 2009;52:5459–71. https://doi.org/10.1016/j.ijheatmasstransfer.2009.06.032.
162. Hetsroni G, Mosyak A, Pogrebnyak E, Sher I, Segal Z. Bubble growth in saturated pool boiling in water and surfactant solution. Int J Multiph Flow. 2006;32:159–82. https://doi.org/10.1016/j.ijmultiphaseflow.2005.10.002.
163. Cattide A, Celata GP, Di Marco P, Grassi W. Experimental study on bubble detachment under variable heat load and the action of electric field. Fluid Dyn Res. 2008;40:485–96. https://doi.org/10.1016/j.fluiddyn.2008.01.003.
164. Ma X, Cheng P, Gong S, Quan X. Mesoscale simulations of saturated pool boiling heat transfer under microgravity conditions. Int J Heat Mass Transf. 2017;114:453–7. https://doi.org/10.1016/j.ijheatmasstransfer.2017.06.019.
165. Zhang L, Shoji M. Nucleation site interaction in pool boiling on the artificial surface. Int J Heat Mass Transf. 2003;46:513–22. https://doi.org/10.1016/S0017-9310(02)00291-0.
166. Nimkar ND, Bhavnani SH, Jaeger RC. Effect of nucleation site spacing on the pool boiling characteristics of a structured surface. Int J Heat Mass Transf. 2006;49:2829–39. https://doi.org/10.1016/j.ijheatmasstransfer.2006.02.018.
167. Hutter C, Sefiane K, Karayiannis TG, Walton AJ, Nelson RA, Kenning DBR. Nucleation site interaction between artificial cavities during nucleate pool boiling on silicon with integrated micro-heater and temperature micro-sensors. Int J Heat Mass Transf. 2012;55:2769–78. https://doi.org/10.1016/j.ijheatmasstransfer.2012.02.014.
168. Golobič I, Gjerkeš H. Interactions between laser-activated nucleation sites in pool boiling. Int J Heat Mass Transf. 2001;44:143–53. https://doi.org/10.1016/S0017-9310(00)00087-9.
169. Akiyama M, Tachibana HON. Effects of system pressure on bubble growth rate. Trans JSME. 1969;35:117–26. https://doi.org/10.3901/CJME.2015.0703.086.
170. Sakashita H. Bubble Growth Rates and Nucleation Site Densities in Saturated Pool Boiling of Water at High Pressures. J Nucl Sci Technol. 2011;48:734–43. https://doi.org/10.1080/18811248.2011.9711756.
171. Lamas MI, Jabardo JMS, Arce A, Fariñas P. Numerical analysis of the bubble detachment diameter in nucleate boiling. Journal of Physics: Conference Series, vol. 395, Institute of Physics Publishing; 2012, p. 12174. https://doi.org/10.1088/1742-6596/395/1/012174.
172. Hutter C, Kenning DBR, Sefiane K, Karayiannis TG, Lin H, Cummins G, et al. Experimental pool boiling investigations of FC-72 on silicon with artificial cavities and integrated temperature microsensors. Exp Therm Fluid Sci. 2010;34:422–33. https://doi.org/10.1016/j.expthermflusci.2009.03.010.
173. Chen HX, Sun Y, Xiao HY, Wang XD. Bubble dynamics and heat transfer characteristics on a micropillar-structured surface with different nucleation site positions. J Therm Anal Calorim. 2020;141:447–64. https://doi.org/10.1007/s10973-020-09301-x.
174. Gupta SK, Misra RD. Effect of two-step electrodeposited Cu–TiO 2 nanocomposite coating on pool boiling heat transfer performance. J Therm Anal Calorim. 2019;136:1781–93. https://doi.org/10.1007/s10973-018-7805-7.
175. Gajghate SS, Barathula S, Das S, Saha BB, Bhaumik S. Experimental investigation and optimization of pool boiling heat transfer enhancement over graphene-coated copper surface. J Therm Anal Calorim. 2020;140:1393–411. https://doi.org/10.1007/s10973-019-08740-5.
176. Das S, Johnsan R, Sujith Kumar CS, Datta A. Experimental study of pool boiling heat transfer on an annealed TiO_2 nanofilm heating surface. J Therm Anal Calorim. 2020. https://doi.org/10.1007/s10973-020-09503-3.
177. Saffari H, Fathalizadeh H, Moghadasi H, Alipour S, Hosseinalipour SM. Experimental study of pool boiling enhancement for surface structuring with inclined intersected mesochannels using WEDM method on copper surfaces. J Therm Anal Calorim. 2020;139:1849–61. https://doi.org/10.1007/s10973-019-08601-1.
178. Nunes JM, de Souza RR, Rodrigues AR, Safaei MR, Cardoso EM. Influence of coated surfaces and gap size on boiling heat transfer of deionized water. J Brazilian Soc Mech Sci Eng. 2020;42:1–14. https://doi.org/10.1007/s40430-020-2223-8.
179. Dong L, Quan X, Cheng P. An experimental investigation of enhanced pool boiling heat transfer from surfaces with micro/nano-structures. Int J Heat Mass Transf. 2014;71:189–96. https://doi.org/10.1016/j.ijheatmasstransfer.2013.11.068.
180. Li C, Wang Z, Wang P-I, Peles Y, Koratkar N, Peterson GP. Nanostructured copper interfaces for enhanced boiling. Small. 2008;4:1084–8. https://doi.org/10.1002/smll.200700991.
181. Park Y, Kim H, Kim J, Kim H. Measurement of liquid-vapor phase distribution on nano- and microstructured boiling surfaces. Int J Multiph Flow. 2016;81:67–76. https://doi.org/10.1016/j.ijmultiphaseflow.2016.01.007.
182. Li S, Furberg R, Toprak MS, Palm B, Muhammed M. Nature-inspired boiling enhancement by novel nanostructured macroporous surfaces. Adv Funct Mater. 2008;18:2215–20. https://doi.org/10.1002/adfm.200701405.
183. Rini DP, Chen RH, Chow LC. Bubble behavior and heat transfer mechanism in FC-72 pool boiling. Exp Heat Transf. 2001;14:27–44. https://doi.org/10.1080/089161501461620.
184. Ramaswamy C, Joshi Y, Nakayama W, Johnson WB. High-speed visualization of boiling from an enhanced structure. Int J Heat Mass Transf. 2002;45:4761–71. https://doi.org/10.1016/S0017-9310(02)00196-5.
185. El-Genk MS, Bostanci H. Saturation boiling of HFE-7100 from a copper surface, simulating a microelectronic chip. Int J Heat Mass Transf. 2003;46:1841–54. https://doi.org/10.1016/S0017-9310(02)00489-1.
186. Demiray F, Kim J. Microscale heat transfer measurements during pool boiling of FC-72: Effect of subcooling. Int J Heat Mass Transf. 2004;47:3257–68. https://doi.org/10.1016/j.ijheatmasstransfer.2004.02.008.
187. Nimkar ND, Bhavnani SH, Jaeger RC. Benchmark heat transfer data for microstructured surfaces for immersion-cooled microelectronics. IEEE Trans Components Packag Technol. 2006;29:89–97. https://doi.org/10.1109/TCAPT.2005.850536.

188. McHale JP, Garimella SV. Measurements of bubble nucleation characteristics in pool boiling of a wetting liquid on smooth and roughened surfaces. 2008 Proceedings of the ASME Heat Transfer Summer Conference HT 2008, vol. 3, 2009, p. 619–29. https://doi.org/10.1115/ht2008-56179.
189. McHale JP, Garimella SV. Nucleate boiling from smooth and rough surfaces - Part 2: Analysis of surface roughness effects on nucleate boiling. Exp Therm Fluid Sci. 2013;44:439–55. https://doi.org/10.1016/j.expthermflusci.2012.08.005.
190. Anderson TM, Mudawar I. Microelectronic cooling by enhanced pool boiling of a dielectric fluorocarbon liquid. J Heat Transfer. 1989;111:752–9. https://doi.org/10.1115/1.3250747.
191. Narumanchi S, Troshko A, Bharathan D, Hassani V. Numerical simulations of nucleate boiling in impinging jets: Applications in power electronics cooling. Int J Heat Mass Transf. 2008;51:1–12. https://doi.org/10.1016/j.ijheatmasstransfer.2007.05.026.
192. Engelberg-Forster K, Greif R. Heat transfer to a boiling liquid—mechanism and correlations. J Heat Transfer. 1959;81:43–52. https://doi.org/10.1115/1.4008129.
193. Ali AF, El-Genk MS. Spreaders for immersion nucleate boiling cooling of a computer chip with a central hot spot. Energy Convers Manag. 2012;53:259–67. https://doi.org/10.1016/j.enconman.2011.09.007.
194. Birbarah P, Gebrael T, Foulkes T, Stillwell A, Moore A, Pilawa-Podgurski R, et al. Water immersion cooling of high power density electronics. Int J Heat Mass Transf. 2020;147:118918. https://doi.org/10.1016/j.ijheatmasstransfer.2019.118918.
195. Gang P, Huide F, Huijuan Z, Jie J. Performance study and parametric analysis of a novel heat pipe PV/T system. Energy. 2012;37:384–95. https://doi.org/10.1016/j.energy.2011.11.017.
196. Jouhara H, Chauhan A, Nannou T, Almahmoud S, Delpech B, Wrobel LC. Heat pipe based systems - Advances and applications. Energy. 2017;128:729–54. https://doi.org/10.1016/j.energy.2017.04.028.
197. Chaudhry HN, Hughes BR, Ghani SA. A review of heat pipe systems for heat recovery and renewable energy applications. Renew Sustain Energy Rev. 2012;16:2249–59. https://doi.org/10.1016/j.rser.2012.01.038.
198. Cui Y, Yu H, Wang H, Wang Z, Yan X. The numerical modeling of the vapor bubble growth on the silicon substrate inside the flat plate heat pipe. Int J Heat Mass Transf. 2020;147:118945. https://doi.org/10.1016/j.ijheatmasstransfer.2019.118945.
199. Kiatsiriroat T, Nuntaphan A, Tiansuwan J. Thermal performance enhancement of thermosyphon heat pipe with binary working fluids. Exp Heat Transf. 2000;13:137–52. https://doi.org/10.1080/089161500269517.
200. Bolozdynya AI, Dmitrenko VV, Efremenko YV, Khromov AV, Shafigullin RR, Shakirov AV, et al. The two-phase closed tubular cryogenic thermosyphon. Int J Heat Mass Transf. 2015;80:159–62. https://doi.org/10.1016/j.ijheatmasstransfer.2014.09.001.
201. Hijikata K, Chen SJ, Tien CL. Non-condensable gas effect on condensation in a two-phase closed thermosyphon. Int J Heat Mass Transf. 1984;27:1319–25. https://doi.org/10.1016/0017-9310(84)90059-0.
202. Lee J, Kim Y, Jeong S. Transient thermodynamic behavior of cryogenic mixed fluid thermosiphon and its cool-down time estimation. Cryogenics (Guildf). 2010;50:352–8. https://doi.org/10.1016/j.cryogenics.2010.02.001.
203. Felder B, Miki M, Deng Z, Tsuzuki K, Shinohara N, Izumi M, et al. Development of a cryogenic helium-neon gas mixture cooling system for use in a Gd-bulk HTS synchronous motor. IEEE Trans Appl Supercond. 2011;21:2213–6. https://doi.org/10.1109/TASC.2010.2101573.
204. Christie R, Robinson D, Plachta D. Design and Operating Characteristics of a Cryogenic Nitrogen Thermosyphon. AIP Conference Proceedings, vol. 710, American Institute of Physics Inc.; 2004, p. 1079–90. https://doi.org/10.1063/1.1774792.
205. Zhou DW, Ma CF. Local jet impingement boiling heat transfer with R113. Heat Mass Transf Und Stoffuebertragung. 2004;40:539–49. https://doi.org/10.1007/s00231-003-0463-7.
206. Wolf DH, Incropera FP, Viskanta R. Jet Impingement Boiling. Adv Heat Transf. 1993;23:1–132. https://doi.org/10.1016/S0065-2717(08)70005-4.
207. Mitsutake Y, Monde M. Ultra high critical heat flux during forced flow boiling heat transfer with an impinging jet. J Heat Transfer. 2003;125:1038–45. https://doi.org/10.1115/1.1621899.
208. Liu ZH, Tong TF, Qiu YH. Critical heat flux of steady boiling for subcooled water jet impingement on the flat stagnation zone. J Heat Transfer. 2004;126:179–83. https://doi.org/10.1115/1.1668054.
209. Ruch MA, Holman JP. Boiling heat transfer to a freon-113 jet impinging upward onto a flat, heated surface. Int J Heat Mass Transf. 1975;18:51–60. https://doi.org/10.1016/0017-9310(75)90007-1.
210. Ma CF, Bergles AE. Jet impingement nucleate boiling. Int J Heat Mass Transf. 1986;29:1095–101. https://doi.org/10.1016/0017-9310(86)90140-7.
211. Bergles E, Ma C-F. Boiling jet impingement cooling of simulated microelectronic chips. Heat transfer in electronic equipment; Proceedings of the Symposium, Boston, MA, November 13–18, 1983
212. Monde M, Katto Y. Burnout in a high heat-flux boiling system with an impinging jet. Int J Heat Mass Transf. 1978;21:295–305. https://doi.org/10.1016/0017-9310(78)90122-9.
213. Katto Y, Kunihiro M. Study of the mechanism of burn-out in boiling system of high burn-out heat flux. Bull JSME. 1973;16:1357–66. https://doi.org/10.1299/jsme1958.16.1357.
214. Wadsworth DC, Mudawar I. Cooling of a multichip electronic module by means of confined two-dimensional jets of dielectric liquid. J Heat Transfer. 1990;112:891–8. https://doi.org/10.1115/1.2910496.
215. Mudawar I, Wadsworth DC. Critical heat flux from a simulated chip to a confined rectangular impinging jet of dielectric liquid. Int J Heat Mass Transf. 1991;34:1465–79. https://doi.org/10.1016/0017-9310(91)90289-Q.
216. Miyasaka Y, Inada S, Owase Y. Critical heat flux and subcooled nucleate boiling in transient region between a two-dimensional water jet and a heated surface. J Chem Eng Japan. 1980;13:29–35. https://doi.org/10.1252/jcej.13.29.
217. Sekoguchi K, Tsutsui M, Nishikawa K, Fukui H. Investigation into the statistical characteristics of bubbles in two-phase flow - 2nd report, the application and establishment of electric resistivity probe method. Bull JSME (Jap Soc Mech Eng). 1975;18:387–404. https://doi.org/10.1299/kikai1938.40.2302.
218. Xie J, Wong TN, Duan F. Modelling on the dynamics of droplet impingement and bubble boiling in spray cooling. Int J Therm Sci. 2016;104:469–79. https://doi.org/10.1016/j.ijthermalsci.2016.02.016.
219. Rini DP, Chen RH, Chow LC. Bubble behavior and nucleate boiling heat transfer in saturated FC-72 spray cooling. J Heat Transfer. 2002;124:63–72. https://doi.org/10.1115/1.1418365.
220. Wang JX, Li YZ, Zhang HS, Wang SN, Mao YF, Zhang YN, et al. Investigation of a spray cooling system with two nozzles for space application. Appl Therm Eng. 2015;89:115–24. https://doi.org/10.1016/j.applthermaleng.2015.05.082.
221. Silk EA, Kim J, Kiger K. Spray cooling of enhanced surfaces: Impact of structured surface geometry and spray axis inclination. Int J Heat Mass Transf. 2006;49:4910–20. https://doi.org/10.1016/j.ijheatmasstransfer.2006.05.031.
222. Elston L, Yerkes K, Thomas S, McQuillen J. Effect of Variable Gravity on the Cooling Performance of a 16-Nozzle Spray Array.

47th AIAA Aerosp. Sci. Meet. Incl. New Horizons Forum Aerosp. Expo., Reston, Virigina: American Institute of Aeronautics and Astronautics; 2009. https://doi.org/10.2514/6.2009-1025.
223. Xie JL, Tan YB, Wong TN, Duan F, Toh KC, Choo KF, et al. Multi-nozzle array spray cooling for large area high power devices in a closed loop system. Int J Heat Mass Transf. 2014;78:1177–86. https://doi.org/10.1016/j.ijheatmasstransfer.2014.07.067.
224. Yan ZB, Toh KC, Duan F, Wong TN, Choo KF, Chan PK, et al. Experimental study of impingement spray cooling for high power devices. Appl Therm Eng. 2010;30:1225–30. https://doi.org/10.1016/j.applthermaleng.2010.02.003.
225. Lin L, Ponnappan R, Yerkes K. Actively pumped two-phase loop for spray cooling. J Thermophys Heat Transf. 2006;20:107–10. https://doi.org/10.2514/1.15053.